Recirculating Foxp3+ regulatory T cells are restimulated in the thymus under Aire control

Jonathan Charaix, Alexia Borelli, Jérémy Santamaria, Lionel Chasson, Matthieu Giraud, Arnauld Sergé, Magali Irla

Recirculating Foxp3$^+$ regulatory T cells are restimulated in the thymus under Aire control

Jonathan Charaix[1*], Alexia Borelli[1*], Jérémy C. Santamaria[1], Lionel Chasson[1], Matthieu Giraud[2], Arnauld Sergé[3] and Magali Irla[1#]

[1] Centre d'Immunologie de Marseille-Luminy, Aix-Marseille University, CNRS, INSERM, CIML, Marseille, France

[2] Center for Research in Transplantation and Translational Immunology, UMR 1064, INSERM, Nantes Université, 44000, Nantes, France

[3] Turing Centre for Living Systems, Laboratoire adhésion inflammation (LAI), CNRS, INSERM, Aix Marseille University, 13288, Marseille, France.

[#]Correspondence: Magali.Irla@inserm.fr

*These two authors contributed equally to this work.

ORCID : Alexia Borelli (0000-0003-2611-7541), Jérémy C. Santamaria (0000-0001-7613-3668), Matthieu Giraud (0000-0002-1208-9677), Arnauld Sergé (0000-0003-4271-3706) et Magali Irla (0000-0001-8803-9708)

Running title:

Recirculating Foxp3$^+$ regulatory T cells are restimulated in the thymus under Aire control

Keywords

Autoimmune regulator; Autoimmunity; Medullary thymic epithelial cells; Foxp3$^+$ Regulatory T cells; Thymus

Abstract

Thymically-derived Foxp3$^+$ regulatory T cells (T_{reg}) critically control immunological tolerance. These cells are generated in the medulla through high affinity interactions with medullary thymic epithelial cells (mTEC) expressing the Autoimmune regulator (Aire). Recent advances have revealed that thymic T_{reg} contain not only developing but also recirculating cells from the periphery. Although Aire is implicated in the generation of Foxp3$^+$ T_{reg}, its role in the biology of recirculating T_{reg} remains elusive. Here, we show that Aire regulates the suppressive signature of recirculating T_{reg} independently of the remodeling of the medullary 3D organization throughout life where T_{reg} reside. Accordingly, the adoptive transfer of peripheral Foxp3$^+$ T_{reg} in *Aire*^{KO} recipients led to an impaired suppressive signature upon their entry into the thymus. Furthermore, recirculating T_{reg} from *Aire*^{KO} mice failed to attenuate the severity of multiorgan autoimmunity, demonstrating that their suppressive function is altered. Using bone marrow chimeras, we reveal that mTEC-specific expression of Aire controls the suppressive signature of recirculating T_{reg}. Finally, mature mTEC lacking *Aire* were inefficient in stimulating peripheral T_{reg} both in polyclonal and antigen-specific co-culture assays. Overall, this study demonstrates that Aire confers to mTEC the ability to restimulate recirculating T_{reg}, unravelling a novel function for this master regulator in T_{reg} biology.

Introduction

$CD25^+Foxp3^+$ regulatory T cells (T_{reg}) constitute a distinct subset of $CD4^+$ T cells endowed with suppressive functions. By maintaining immune tolerance, T_{reg} critically prevent the emergence of autoimmune and inflammatory diseases. The vast majority of T_{reg} is produced in the thymic medulla where they arise from two distinct developmental programs involving $CD25^+Foxp3^-$ ($CD25^+$ T_{reg}P) and $CD25^-Foxp3^{lo}$ ($Foxp3^{lo}$ T_{reg}P) precursors (1-4). For a long-time, thymic $CD25^+Foxp3^+$ T_{reg} were thought to exclusively correspond to developing cells. However, recent studies have shown that circulating $CD25^+Foxp3^+$ T_{reg} have the ability to migrate back into the thymus (5-7). Thus, thymic $CD25^+Foxp3^+$ T_{reg} is a heterogeneous population containing both developing and recirculating cells (3). Interestingly, recirculating T_{reg} show suppressive properties similar to their splenic counterparts (7). They exhibit an activated and differentiated phenotype and were found to negatively regulate the *de novo* generation of $CD25^+Foxp3^+$ T_{reg} through IL-2 consumption (5).

The recirculation of peripheral $Foxp3^+$ T_{reg} in the thymus is mediated at least by two chemokine receptors, CCR6 and CXCR4 (5, 8). Interestingly, the entry of peripheral *Ccr6*$^{-/-}$ T_{reg} into the thymus is impaired, suggesting that CCR6, expressed by effector/memory T cells, is involved in the recirculation of $Foxp3^+$ T_{reg} from the periphery to this organ (8). Furthermore, the expression of the CCR6 ligand, CCL20, is regulated by the Autoimmune regulator (Aire) (8). Aire is mainly expressed by a subset of medullary thymic epithelial cells (mTEC) commonly called $mTEC^{hi}$, characterized by a $CD80^{hi}MHCII^{hi}$ phenotype. Furthermore, upon recirculation into the thymus, a subset of B cells has been described to upregulate Aire (9). Independent reports have described that $CD25^+Foxp3^+$ T_{reg} are reduced in the thymus of *Aire*^{KO} mice (10, 11). Accordingly, *Aire* expression was proposed to direct autoreactive $CD4^+$ thymocytes into the T_{reg} cell lineage (12). Interestingly, in the perinatal life, Aire promotes the generation of a distinct population of $Foxp3^+$ T_{reg}, which persists in adults and prevents the emergence of autoimmunity (13). In C57BL/6 mice, *Aire*-deficiency is associated with mild autoimmunity characterized by lymphocyte infiltrations and autoantibody production targeting several organs such as the pancreas, eyes, salivary glands, liver and lungs (14-17). In human, autosomal recessive mutations in the *Aire* gene induce a life threatening pathology called autoimmune polyendocrinopathy-candidiasis-ectodermal dystrophy (APECED), also known as autoimmune polyendocrine syndrome-type 1 (APS-1) (18, 19). Interestingly, numbers, activation and suppressive functions of $Foxp3^+$ T_{reg} are altered in APECED patients (20-22).

Although thymic $Foxp3^+$ T_{reg} have been found to be more heterogeneous than previously thought (3), this emerging population of recirculating peripheral T_{reg} remains poorly described. In particular, the mechanisms that control

their suppressive phenotype in the thymus are unknown. In this study, we show that Aire regulates the suppressive properties of recirculating CCR6$^+$ T_{reg}, independently of the remodeling of the 3D organization of the thymic medulla where they reside (5). High-throughput sequencing revealed that recirculating CCR6$^+$ T_{reg} in the thymus of *Aire*^{KO} mice have impaired expression of several genes associated with T_{reg} suppressive functions and helper T cell polarization. Accordingly, recirculating CCR6$^+$ T_{reg} from *Aire*^{KO} mice failed to attenuate the severity of multi-organ autoimmunity, demonstrating that their suppressive activity is impaired. Moreover, the adoptive transfer of splenic Foxp3$^+$ T_{reg} in *Aire*^{KO} recipients resulted in an impaired suppressive signature upon their recirculation in the thymus. By using bone marrow (BM) chimeras, we demonstrate that *Aire* expressed by mTEC rather than by thymic B cells is responsible for the suppressive properties of recirculating CCR6$^+$ T_{reg}. Finally, recirculating T_{reg} were found in close contact with Aire$^+$ mTEC and restimulated in an antigen-specific manner. Altogether, our data reveal that Aire confers to mTEC the capacity to control the restimulation of recirculating CCR6$^+$ T_{reg} in the thymus.

Materials and methods

Mice

CD45.1 WT (B6.SJL-*PtprcaPepcb*/BoyCrl, Stock n°002014, Charles River), CD45.2 WT (Stock n°000664, Charles River), CD45.1/2 WT, CD45.2 *Aire*^{KO} (23), *Rag2*^{KO} (24), CD45.1 Foxp3^{eGFP} mice (25), OTII (26) and Rip-mOVA (27) were on a C57BL/6J background. Rip-mOVA x OTII mice were backcrossed on a *Rag2*^{KO} background. All mice were maintained under specific pathogen-free conditions at the Centre d'Immunologie de Marseille-Luminy (CIML, France). Standard food and water were given *ad libitum*. Males and females were used at the age of 5 days, 9 days, 6 weeks and 1 year. Chimeras were generated between 6 to 10 weeks of age. All experiments were done in accordance with national and European laws for laboratory animal welfare (EEC Council Directive 2010/63/UE) and the Marseille Ethical Committee for Animal experimentation no. 14.

BM chimeras

BM chimeras were generated by injecting intravenously (*i.v.*) 5.10^6 BM cells from CD45.1 Foxp3^{eGFP} mice into lethally irradiated CD45.2 *Aire*^{WT} or *Aire*^{KO} recipients (two doses of 500 rads, 8h apart, X-ray using a RS-2 000 Irradiator; Rad Source Technologies). Similarly, 5.10^6 BM cells from either CD45.2 *Aire*^{WT} or *Aire*^{KO} mice were injected into lethally irradiated CD45.1/2 WT recipients. Mice were analyzed 6 weeks post-reconstitution.

Foxp3$^+$ T_{reg} adoptive transfer

5.10^5 cell-sorted splenic congenic CD45.1 $CD4^+CD25^+Foxp3^{eGFP}$ T_{reg} were *i.v* injected into sublethally irradiated CD45.2 $Aire^{WT}$ or $Aire^{KO}$ recipient mice (one dose of 500 rads, X-ray using a RS-2 000 Irradiator; Rad Source Technologies). Mice were analyzed 1-week post-T_{reg} adoptive transfer.

Multi-organ autoimmunity experiments

Rag2^{KO} recipients were injected *i.v.* with 3.10^6 $CD4^+CD25^+$ T_{reg}-depleted splenocytes purified from CD45.1 WT mice. Four weeks later, 15.10^4 splenic $CD4^+CD25^{hi}$ T_{reg} or 10.10^4 recirculating thymic $CCR6^+CD4^+CD25^+$ T_{reg} from $Aire^{WT}$ or $Aire^{KO}$ mice were adoptively transferred. Mice that did not receive any T_{reg} were used as controls. Peripheral tissues were harvested and analyzed three weeks later.

Cell isolation

Thymic T_{reg}, splenic T_{reg} and T_{reg}-depleted splenocytes were isolated by scratching the thymus or the spleen on a 70-µm mesh. Red blood cells were lysed with RBC lysis buffer (eBioscience). Thymic and splenic T_{reg} cells were pre-enriched by depleting $CD8^+$ and $CD19^+$ cells using biotinylated anti-CD8α (clone 53.6.7; BD Biosciences) and anti-CD19 (clone 1D3; BD Bioscience) antibodies with anti-biotin microbeads by AutoMACS using the Deplete program (Miltenyi Biotech). Recirculating thymic T_{reg} were sorted as $CCR6^+CD4^+CD8^-CD25^+$ cells and splenic T_{reg} as $CD4^+CD25^{hi}$ cells using a FACSAria III cell sorter (BD Biosciences). Splenocytes were depleted of $CD4^+CD25^+$ T_{reg} using a FACSAria III cell sorter (BD Biosciences). Thymus were digested at 37°C in HBSS medium containing Liberase TM (50 µg/ml; Roche) and DNase I (100 µg/ml; Roche) until complete tissue digestion. Total mTEC ($CD45^-EpCAM^+UEA\text{-}1^+Ly51^{-/lo}$) or $mTEC^{hi}$ ($CD45^-EpCAM^+UEA\text{-}1^+Ly51^{-/lo}CD80^{hi}$) were pre-enriched by depleting CD45 hematopoietic cells using anti-CD45 magnetic beads (Miltenyi Biotec) by AutoMACS with the DepleteS program and sorted using a FACSAria III cell sorter (BD Biosciences).

***In vitro* co-culture assays**

3.10^4 cell-sorted splenic $CD4^+CD25^{hi}$ T_{reg} from $Aire^{WT}$ or $Aire^{KO}$ mice were co-cultured for 24h with 6.10^3 $CD45^-EpCAM^+UEA\text{-}1^+Ly51^{-/lo}$ mTEC from $Aire^{WT}$ or $Aire^{KO}$ mice in RPMI (ThermoFisher) supplemented with 10% FBS (Sigma Aldrich), L-glutamine (2 mM, ThermoFisher), sodium pyruvate (1 mM, ThermoFisher), 2-mercaptoethanol (2×10^{-5} M, ThermoFisher), penicillin (100 IU per ml, ThermoFisher), streptomycin (100 µg per ml, ThermoFisher) and mouse IL-2 (40 ng/ml, Immunotools). For antigen-specific co-culture assays, 5.10^3 cell-sorted splenic $CD4^+CD25^{hi}$ T_{reg} from Rip-mOVA x OTII x *Rag2*^{KO} mice were co-cultured for 24h with 1.10^3 $CD45^-EpCAM^+Ly51^{-/lo}Aire^{eGFP}$ mTEC from $Aire^{het}$ or $Aire^{KO}$ mice previously loaded with $OVA_{323\text{-}339}$ peptide (5µg/ml, Polypeptide group) for 2h.

Flow cytometry

Cells were stained with standard procedures using antibodies listed in Table S2. For intracellular staining with anti-Foxp3, anti-GITRL and anti-OX40L antibodies, cells were fixed, permeabilized and stained with the Foxp3 staining kit according to the manufacturer's instructions (eBioscience). Stained cells were analyzed with FACSCanto II and LSR II (BD Biosciences) and data were analyzed using FlowJo software (Tree Star).

Quantitative RT-PCR

Total RNA was extracted with TRIzol (Invitrogen) and cDNA was synthesized with random oligo dT primers and Superscript II reverse transcriptase (Invitrogen). Quantitative PCR was performed with SYBR Premix Ex Taq Master Mix (Takara) on an ABI 7500 fast real-time PCR system (Applied Biosystem). The results were normalized to actin mRNA expression. A list of primer sequences is provided in Table S3.

RNA-sequencing experiments

5.10^4 $CCR6^+$ T_{reg} were cell-sorted from the thymus of 6 week-old *Aire*^{WT} and *Aire*^{KO} mice. Two biological replicates were prepared for each condition. The total RNA was extracted using the RNeasy Micro Kit (Qiagen) and treated with DNase I. RNA-seq libraries were prepared using the TruSeq Stranded mRNA kit (Illumina) and sequenced with the Illumina HiSeq 2000 machine to generate datasets of single-end 50bp reads. The reads were mapped to the mouse reference genome (mm10) using TopHat2 (version 2.0.12) (28), then counted using Cufflinks or Cuffdiff (version 2.2.1) (29, 30) and the mm10 genome GTF gene annotation file. In addition to read counting, Cuffdiff performs between-sample normalization and was used to calculate the differential gene expression and its statistical significance in *Aire*^{WT} vs *Aire*^{KO} T_{reg} by using the default "pooled" dispersion method that applies to experiments having few (≥2) biological replicates per condition. Expression levels generated by Cufflinks, as fragments per kilobase of transcript per million mapped reads (FPKM), were processed by the Matrix2png program (31) to generate heatmaps of gene expression levels. The dataset generated in this study are available in the Gene Expression Omnibus (GEO) database under accession number GSE188419. The expression of *Tnfsf4* and *Tnfsf18* was analyzed in RNA-sequencing dataset from *Aire*^{KO} mTEC^{hi} (GSE87133).

Immunofluorescence staining

Thymi were collected from 9 day-, 6 week- and 1 year-old *Aire*^{WT} or *Aire*^{KO} mice and fat tissues removed to avoid any interference with the 3D reconstitution process. Organs were longitudinally included in O.C.T (Sakura Finetek), frozen at -80 °C and cut in 20-µm-thick slices. Thymic sections were fixed with 2% paraformaldehyde, then saturated with 3% BSA and 0.01% Triton X100 in 0.1 M Tris HCl buffer. Sections were next stained for 45

min with rabbit anti-keratin 14 or with anti-Aire Alexa Fluor 488 (5H12; eBioscience), anti-Foxp3 PE (FJK-16s; eBioscience) and anti-CD73 Alexa Fluor 647 (TY/11.8; Biolegend) in hybridization buffer (1% BSA and 0.02% Triton X100 in 0.1 M Tris HCl, pH 7.4). Keratin 14 staining was revealed with Cy3-conjugated anti-rabbit (Invitrogen). Sections were counterstained with DAPI (1 µL/mL, BioLegend) and mounted with Mowiol (Calbiochem). For 3D reconstruction, images were acquired with a slide scanner (Panoramic SCAN II; 3D Histech). Confocal microscopy was performed with a LSM 780 confocal microscope (Carl Zeiss Microscopy).

Detection of immune infiltrates and autoantibodies

Peripheral tissues were fixed in buffered 10% formalin solution. 4 µm-thick paraffin-embedded sections were counterstained with hematoxylin and eosin. Autoantibody production was assessed by immunostaining organ sections from *Rag2*^{KO} mice with the sera (1/80) of analyzed mice. Autoantibodies were revealed with FITC-conjugated goat anti-mouse IgG. Sections were counterstained with DAPI and mounted with Mowiol (Calbiochem). All images were acquired with a slide scanner (Panoramic SCAN II; 3D Histech) and analyzed with ImageJ software (National Institutes of Health) to compute the mean fluorescence intensity of each image.

3D reconstitution

For 3D reconstitution, images from the entire thymus of 9 day-, 6 week- and 1-year-old *Aire*^{WT} and *Aire*^{KO} mice were processed with For3D software as previously described (32, 33). Briefly, images were smoothed by median and Gaussian filtering and medulla volumes were determined using ImageJ and Matlab (The Mathworks) software. Medullary islets identified in the 3D structures were measured individually using ImageJ and were color-coded using Imaris (Bitplane).

Statistical analysis

Statistics were performed with GraphPad Prism 9.1 software. Normal distribution of the data was assessed using d'Agostino-Pearson omnibus normality test. Statistical significance was then assessed using unpaired Student's *t* test for two normal distributions, Mann-Whitney test for two non-normal distributions or Kruskal-Wallis test for more than two distributions. *$p < 0.05$; **$p < 0.01$; ***$p < 0.001$, ****$p < 0.0001$. All bar graphs show mean ± SEM, unless mentioned.

Results

Aire regulates the recirculation of peripheral CD25$^+$Foxp3$^+$ T$_{reg}$ in the thymus, independently of the remodeling of the 3D organization of the medulla throughout life

Considering the importance of Aire in the induction of self-tolerance (34), we first assessed whether it could be involved in the topology of the thymic medulla. For this, we compared WT (*Aire*^{WT} mice) with *Aire*-deficient mice in which the first exon of the *Aire* locus was replaced by the sequence of enhanced green fluorescent protein (eGFP) (*Aire*^{KO} mice) (23). Thymic sections of 9 day-, 6 week- and 1-year-old, either *Aire*^{WT} or *Aire*^{KO} mice were stained with the keratin-14 mTEC-specific marker (35) and reconstructed with our in-house dedicated "Full organ reconstruction in 3D" (For3D) software (33) (**Fig. 1A-C and Movies S1-6**). Interestingly, the number of medullary islets in *Aire*^{WT} mice diminished between 9 days and 6 weeks of age while it increased between 6 weeks and 1 year of age (**Fig. 1D)**. Furthermore, the total and individual medullary volumes increased between 9 days and 6 weeks while it decreased between 6 weeks and 1 year (**Fig. 1E,F)**. Nevertheless, the central compartment of ~1 mm^3 was observed at all ages analyzed (**Fig. 1F)** These observations reveal that the medulla organization is dynamic throughout life. In comparison to *Aire*^{WT} mice, the thymi of *Aire*^{KO} mice show a similar dynamic medulla organization characterized by normal numbers of medullary islets and total medullary volumes with the presence of a major compartment (**Fig. 1A-C,F)**. These results indicate that the dynamic remodeling of the 3D organization of the thymic medulla throughout life is not regulated by Aire.

Because medulla formation correlates with Foxp3$^+$ T$_{reg}$ emergence during ontogeny (36), we next analyzed whether *Aire* deficiency could affect their development in neonates of 5 days of age. In contrast to CD25$^+$ T$_{reg}$P, frequencies and numbers of Foxp3^{lo} T$_{reg}$P and mature CD25$^+$Foxp3$^+$ T$_{reg}$ were diminished in the thymus of 5-day-old *Aire*^{KO} mice compared to their respective counterparts (**Fig. 2A)**. This decrease was also observed in 6-week- and 1-year-old *Aire*^{KO} mice (**Fig. 2B,C**). Since mature CD25$^+$Foxp3$^+$ T$_{reg}$ contain both developing and recirculating cells in the adult thymus, we used the key thymus-homing chemokine receptor CCR6 to distinguish developing (CCR6$^-$) and recirculating (CCR6$^+$) mature T$_{reg}$ (6). Interestingly, both numbers of CCR6$^-$ and CCR6$^+$ mature T$_{reg}$ were reduced in *Aire*^{KO} mice compared to *Aire*^{WT} mice at 6 weeks and 1 year of age (**Fig. 2D,E**). Furthermore, 1-year-old *Aire*^{WT} mice showed a marked reduction in numbers of CCR6$^-$ and CCR6$^+$ mature CD25$^+$Foxp3$^+$ T$_{reg}$ compared to 6-week-old *Aire*^{WT} mice, which reflects the effect of thymic involution on T$_{reg}$ cells in normal conditions. To date, two chemokine receptors, CCR6 and CXCR4 have been implicated in the recirculation of peripheral T$_{reg}$ into the thymus (5, 8). Strikingly, the expression of their respective ligands, *Ccl20* and *Cxcl12*, was

substantially reduced in *Aire*^{KO} mTEC^{hi} (**Fig. 2F**), consistently with the altered recirculation of peripheral T_{reg} in the thymus. Altogether, these results show that Aire controls both the development and recirculation of Foxp3^{+} T_{reg} throughout life.

Thymic CCR6^{+} T_{reg} from *Aire*^{KO} mice show an impaired effector and suppressive phenotype

Because Aire controls the recirculation of CCR6^{+} T_{reg}, we made the hypothesis that it could also control their suppressive properties. To test this hypothesis, we first measured the expression level of several genes associated with T_{reg} suppressive functions in purified CCR6^{+}CD4^{+}CD25^{+} single-positive (SP) thymocytes that correspond to CD25^{+}Foxp3^{+} T_{reg} (**Fig. S1**). Interestingly, whereas *Foxp3* level was normal, the expression of *Klrg1*, a marker of terminally differentiated T_{reg} (37), was reduced in CCR6^{+} T_{reg} from 6-week-old *Aire*^{KO} mice (**Fig. 3A**). Accordingly, the expression of genes encoding for the inhibitory cytokine *Il10*, the cytolytic molecules *Gzmb* and *Fasl*, *Lag3*-associated with dendritic cell modulation, as well as the ectoenzymes *Entpd1* (CD39) and *Nt5e* (CD73), implicated in target cell metabolic disruption, was reduced in CCR6^{+} T_{reg} of *Aire*^{KO} mice. A similar altered suppressive signature was also observed in CCR6^{+} T_{reg} purified from the thymus of 1-year-old *Aire*^{KO} mice (**Fig. S2**).

To further determine the impact of Aire on the functional properties of CCR6^{+} T_{reg}, we analyzed their gene expression profile by high-throughput RNA-sequencing (**Fig. 3B,C**). Genes showing a significant variation ($p \leq 0.05$) in gene expression between *Aire*^{WT} and *Aire*^{KO} CCR6^{+} T_{reg} with a fold change difference > 2 or < 0.5 were considered as up- and down-regulated, respectively. We identified a total of 2 634 upregulated genes reaching significance for 1 060 of them (Cuffdiff $p < 0.05$) in *Aire*^{WT} CCR6^{+} T_{reg} compared to their *Aire*^{KO} counterparts (**Fig. 3B**). Moreover, only 1 175 genes were downregulated with 301 of them reaching significance (Cuffdiff $p < 0.05$). Thus, the expression of *Aire* in the thymus upregulates three times more genes than it downregulates in recirculating CCR6^{+} T_{reg}. In accordance with the altered T_{reg} suppressive signature observed by qPCR (**Fig. 3A**), we found that *Il10*, *Gzmb*, *Fasl*, *Lag3*, *Entpd1* and *Nt5e* were downregulated in CCR6^{+} T_{reg} of *Aire*^{KO} mice (**Fig. 3C** and **Table S1**). Furthermore, the expression of *Prdm1* (Blimp-1), which characterizes effector Th-like T_{reg} (38) and the terminally differentiated markers *Klrg1* and *Tigit* (37, 39) was reduced in CCR6^{+} T_{reg} of *Aire*^{KO} mice compared to their *Aire*^{WT} counterparts. Strikingly, CCR6^{+} T_{reg} of *Aire*^{KO} mice also expressed lower levels of several genes associated with their suppressive signature such as *Ctla4* and *Lgals1* (galectin-1) implicated respectively in dendritic cell modulation and target cell apoptosis (40, 41). The expression of *Tbx21* and *Irf4*, encoding for transcription factors associated with Th1- and Th2-like T_{reg}, as well as *Pparg* and *Id2* genes associated with fat-

resident effector T_{reg} (42) was also diminished. Accordingly, the expression of the chemokine receptors *Cxcr3* of Th1-like, *Ccr4* and *Ccr8* of Th2-like as well as *Ccr1* and *Ccr2* of fat-resident T_{reg} (43), implicated in effector T_{reg} migration to the inflammatory site, was reduced in $CCR6^+$ $Aire^{KO}$ T_{reg}. Altogether, these results indicate that *Aire* expression is crucial for the effector and suppressive properties of recirculating $CCR6^+$ T_{reg} in the thymus.

Recirculating $CCR6^+$ T_{reg} from $Aire^{KO}$ mice fail to attenuate the severity of multi-organ autoimmunity

Because numbers and suppressive signature of recirculating $CCR6^+$ T_{reg} were reduced in the thymus of $Aire^{KO}$ mice, we analyzed whether these defects would be also observed in the periphery. Blood and splenic $CD4^+Foxp3^+$ T_{reg} from 6-week- and 1-year-old $Aire^{KO}$ mice showed similar frequencies, numbers and expression levels of suppressive genes compared to their $Aire^{WT}$ counterparts (**Fig. S3**). We next assessed the ability of peripheral and thymic $CCR6^+$ T_{reg} from $Aire^{KO}$ mice to dampen the severity of multiorgan autoimmunity. To this end, $CD4^+CD25^+$ T_{reg}-depleted splenocytes from CD45.1 WT mice were transferred into $Rag2^{KO}$ lymphopenic recipients. Four weeks later, splenic T_{reg} or thymic $CCR6^+$ T_{reg} purified from either $Aire^{WT}$ or $Aire^{KO}$ mice were adoptively transferred into these recipients (**Fig. 4A and Fig. S4A**). Signs of autoimmunity in peripheral tissues were visualized by histology and quantified by flow cytometry three weeks later. $Rag2^{KO}$ mice that did not receive any T_{reg} were used as controls. Accordingly with the normal suppressive signature of splenic T_{reg} from $Aire^{KO}$ mice (**Fig. S3**), $Rag2^{KO}$ mice adoptively transferred with these cells show tissue infiltration levels similar to mice transferred with $Aire^{WT}$ splenic T_{reg} (**Fig. 4B,C**)**.** In marked contrast to mice that received $Aire^{WT}$ thymic $CCR6^+$ T_{reg}, mice adoptively transferred with thymic $CCR6^+$ T_{reg} from $Aire^{KO}$ mice failed to attenuate T-cell infiltration in several peripheral tissues despite similar numbers of CD45.2 donor $Foxp3^+$ T_{reg} in lymph nodes (**Fig. 4D,E and Fig. S4B,C**). Examination of CD45.1 donor cell infiltration by flow cytometry revealed that 100% of $Rag2^{KO}$ mice that received $Aire^{KO}$ thymic $CCR6^+$ T_{reg} showed a high infiltration level in the pancreas and salivary glands, 83% in eyes, 33% in the lung and liver as well as 16% in the kidney (**Fig. 4E**). In contrast, only 16% of $Rag2^{KO}$ mice transferred with $Aire^{WT}$ thymic $CCR6^+$ T_{reg} showed a high infiltration in the liver. Furthermore, flow cytometry analysis showed that thymic $CCR6^+$ T_{reg} of $Aire^{KO}$ mice were unable to prevent the infiltration of CD45.1 $CD4^+$ and $CD8^+$ T cells in the pancreas and eyes as well as CD45.1 $CD8^+$ T cells in salivary glands (**Fig. S4D**). Finally, immunostaining of $Rag2^{KO}$ tissue sections with sera from these mice revealed higher levels of autoantibodies against the pancreas and salivary glands in mice transferred with $Aire^{KO}$ thymic $CCR6^+$ T_{reg} than in mice injected with $Aire^{WT}$ thymic $CCR6^+$ T_{reg} (**Fig. 4F,G**). Thus, thymic $CCR6^+$ T_{reg} of $Aire^{KO}$ mice failed to attenuate the severity of multiorgan autoimmunity, demonstrating that their suppressive activity was impaired.

Aire expression in the thymic stroma controls the suppressive signature of recirculating CCR6$^+$ T$_{reg}$

Since *Aire* expression is not restricted to mTEC but was also found in thymic B cells (9), we then investigated its respective contribution in the stromal and hematopoietic compartments to control the recirculation and suppressive properties of CCR6$^+$ T$_{reg}$. To determine the role of Aire in hematopoietic cells, we generated BM chimeras by reconstituting lethally irradiated CD45.1/2 WT recipients with either CD45.2 *Aire*^{WT} or *Aire*^{KO} BM cells (**Fig. S5A**). Six weeks later, *Aire*^{KO} BM chimeras did not show major defects in total CD19$^+$B220$^+$ B cells, neither in the IgD$^-$ and IgD$^+$ B cell subsets, both described to express Aire (9) (**Fig. S5B,C**). Overall, frequencies and numbers of CD25$^+$ T$_{reg}$P, Foxp3^{lo} T$_{reg}$P, CCR6$^-$ and CCR6$^+$ mature CD25$^+$Foxp3$^+$ T$_{reg}$ were also normal (**Fig. S5D,E**). We next cell-sorted CCR6$^+$ T$_{reg}$ from the thymus of these BM chimeras and analyzed their suppressive signature. Recirculating T$_{reg}$ from both chimeras exhibited a similar expression of suppressive genes that was altered in CCR6$^+$ T$_{reg}$ of *Aire*^{KO} mice (**Fig. S5F**). Thus, *Aire* expression in thymic B cells is unlikely involved in T$_{reg}$ development, recirculation and suppressive signature.

We then analyzed whether *Aire* expression in stromal cells controls CCR6$^+$ T$_{reg}$ functional suppressive properties. To this end, we generated BM chimeras in which lethally irradiated CD45.2 *Aire*^{WT} or *Aire*^{KO} mice were reconstituted with CD45.1 Foxp3^{eGFP} BM cells (**Fig. 5A**). Six weeks later, similar numbers of CD4$^+$ SP thymocytes of CD45.1 donor origin were observed in *Aire*^{WT} and *Aire*^{KO} recipients (**Fig. 5B**). Although numbers of CD25$^+$ T$_{reg}$P and Foxp3^{lo} T$_{reg}$P were also similar in both groups, frequencies and numbers of mature CD25$^+$Foxp3$^+$ T$_{reg}$ were specifically reduced in *Aire*^{KO} chimeras (**Fig. 5C**). This defect was attributable to diminished frequencies and numbers of CCR6$^+$ T$_{reg}$ (**Fig. 5D**). Recirculating CCR6$^+$ mature CD25$^+$Foxp3$^+$ T$_{reg}$ of CD45.1 origin were then cell-sorted from the thymus of both chimeras and analyzed for the expression of several genes associated with T$_{reg}$ effector functions. Whereas *Foxp3* level was normal, the expression of *Klrg1*, *Il10*, *Tgfb1*, *Gzmb*, *Fasl*, *Lag3*, *Entpd1* and *Nt5e* was reduced in *Aire*^{KO} chimeras compared to control chimeras (**Fig. 5E**). Altogether, these results show that whereas *Aire* in hematopoietic cells is dispensable, its specific expression in stromal cells controls both recirculation and suppressive properties of CCR6$^+$ T$_{reg}$.

Antigen-specific restimulation of recirculating T$_{reg}$ by Aire$^+$ mTEC

To further decipher the impact of *Aire*-expressing mTEC in the suppressive signature of recirculating T$_{reg}$, we used an *in vitro* co-culture setup of peripheral T$_{reg}$ and mTEC purified from *Aire*^{WT} or *Aire*^{KO} mice. Compared to *Aire*^{WT} splenic T$_{reg}$ co-cultured with *Aire*^{WT} mTEC, the expression of *Tgfb1*, *Gzmb*, *Fasl*, *Entpd1* and *Nt5e* was reduced in *Aire*^{WT} splenic T$_{reg}$ co-cultured with *Aire*^{KO} mTEC (**Fig. 6A**). Moreover, *Aire*^{KO} splenic T$_{reg}$ co-cultured with

Aire^{WT} mTEC upregulated the expression of these genes in contrast to *Aire*^{KO} splenic T_{reg} co-cultured with *Aire*^{KO} mTEC. Thus, as compared to their *Aire*^{WT} counterparts, *Aire*^{KO} mTEC failed to enhance suppressive signatures of both *Aire*^{WT} and *Aire*^{KO} splenic T_{reg}.

We then analyzed the *in vivo* effect of the *Aire*^{KO} thymic stroma in regulating the suppressive signature of peripheral WT T_{reg}. To this end, splenic T_{reg} purified from CD45.1 Foxp3^{eGFP} congenic mice were adoptively transferred into either *Aire*^{WT} or *Aire*^{KO} recipients (**Fig. 6B).** One week later, we observed reduced frequencies and numbers of donor CD45.1 Foxp3^{eGFP} T_{reg} in the thymus of *Aire*^{KO} mice as compared to *Aire*^{WT} mice (**Fig. 6C).** Moreover, the remaining donor Foxp3^{eGFP} T_{reg} that recirculated back to the thymus exhibited an impaired suppressive signature (**Fig. 6D).** These results not only confirm that Aire favors the recirculation of peripheral T_{reg} in the thymus but also highlight its key role in enhancing their suppressive properties.

Thus, we made the hypothesis that recirculating T_{reg} could be restimulated by Aire^{+} mTEC. To test this, WT thymic sections were first stained for Aire, Foxp3 and CD73, the latter being a reliable marker of recirculating T_{reg} (1, 44). Of note, anti-CCR6 antibody was not used in this experiment because it failed to give any signal in our hands. Interestingly, we observed that both developing CD73^{-} and recirculating CD73^{+} T_{reg} were found in close proximity to Aire^{+} mTEC (**Fig. 6E).** These results suggest that recirculating T_{reg} could be restimulated by establishing antigen-specific contacts with Aire^{+} mTEC. To test this hypothesis, splenic OTII T_{reg} from Rip-mOVA x OTII mice were co-cultured with $OVA_{323-339}$-loaded *Aire*^{het} (*Aire*$^{eGFP/WT}$) or *Aire*^{KO} (*Aire*$^{eGFP/eGFP}$) mTEC^{hi} (**Figure S6**). Compared to unstimulated OVA-specific T_{reg}, *Aire*^{KO} mTEC^{hi} were able to activate OTII T_{reg} but to a lesser extent than *Aire*^{het} mTEC^{hi} (**Fig. 6F).** These results demonstrate that Aire^{+} mTEC can stimulate peripheral T_{reg} in an antigen-specific manner and this ability is impaired in the absence of Aire. Furthermore, as compared to OTII T_{reg} co-cultured with *Aire*^{het} mTEC^{hi}, the expression of *Il10*, *Tgfb1*, *Gzmb*, *Fasl*, *Lag3*, *Entpd1* and *Nt5e* was reduced in OTII T_{reg} co-cultured with *Aire*^{KO} mTEC^{hi} (**Fig. 6G)**, indicating that this antigen-specific restimulation is much less efficient. We thus analyzed MHCII expression in mTEC from *Aire*^{KO} mice. In accordance with a previous study (45) and the pro-apoptotic role of Aire (46), we found increased frequencies of MHCII^{+} mTEC in these mice (**Fig. S7A**). We then made the hypothesis that costimulatory signals may be implicated in the phenotype observed. Two ligands of the Tumor Necrosis Factor Superfamily (TNFSF) have been described to be constitutively expressed by mTEC and participate in thymic T_{reg} development (47). Interestingly, we found that mTEC^{hi} expressed reduced levels of *Tnfsf4* (OX40L, *Aire*^{WT}: 2.32 FPKM vs *Aire*^{KO}: 0.37) and *Tnfsf18* (GITRL, *Aire*^{WT}: 2.92 vs *Aire*^{KO}: 0.81) in *Aire*^{KO} mice (**Fig. S7B**). This result was also confirmed at the protein level by flow cytometry (**Fig. S7C**). These observations are consistent with the reduced cellularity of Foxp3^{lo} T_{reg}P and

CD25^{+}Foxp3^{+} T_{reg} in *Aire*^{KO} mice (**Fig. 2A-C**). Further investigations are needed to decipher the role of these two TNFSF ligands in the biology of recirculating T_{reg} in the thymus. Altogether, our data reveal that Aire^{+} mTEC, through antigen-specific restimulation, are responsible for the strong suppressive signature of recirculating T_{reg}.

Discussion

Our study demonstrates that Aire expression by mTEC promotes the suppressive properties of recirculating CCR6^{+} T_{reg} independently of the dynamic remodeling of the medullary 3D organization, where recirculating T_{reg} reside. We previously described that the medulla of 6-week-old young adult mice is complex with a large central compartment surrounded by hundreds of individual islets (32). Nevertheless, determining whether this topology varies throughout life and whether Aire is implicated remained open issues. Interestingly, we found that 9-day- and 6-week-old WT mice show ~1 000 and ~400 medullary islets, respectively. Given that individual islets arise from a single progenitor (48), these observations suggest that during thymic development, they grow and fuse together, leading to a reduced number of islets in young adult mice compared to neonates. In 1-year-old mice, the number of medullary islets increases to reach ~1 000 islets, as observed in neonates. Considering that the medulla topology is governed by crosstalk with autoreactive CD4^{+} thymocytes (32, 49-52), the high islet number observed in aged mice could be due to a suboptimal cellular crosstalk due to reduced cellularity of CD4^{+} thymocytes linked to age-related thymic involution. Although Aire plays multiple roles in T-cell tolerance induction (34), our results show that it does not shape the 3D organization of the thymic medulla. This is consistent with the fact that the clonal deletion of autoreactive CD4^{+} thymocytes is impaired in *Aire*^{KO} mice (45, 53), which consequently leads to an effective medulla organization.

Several studies have shown that mTEC are implicated in Foxp3^{+} T_{reg} development (54-56). Nevertheless, the specific role of Aire in thymic T_{reg} heterogeneity throughout life remained to be defined. Interestingly, we found that Aire controls the cellularity of Foxp3^{lo} T_{reg}P and mature CD25^{+}Foxp3^{+} T_{reg} in 5-day-, 6-week- and 1-year-old mice. This is illustrated by decreased numbers of Foxp3^{lo} T_{reg}P and CD25^{+}Foxp3^{+} T_{reg} in *Aire*^{KO} mice, which could not be due to impaired medulla organization since no defect was observed at this level. Given that CD25^{+} T_{reg}P and Foxp3^{lo} T_{reg}P show distinct developmental pathways that give rise to CD25^{+}Foxp3^{+} T_{reg} with non-overlapping regulatory activities (1), our results provide new insights in the role of Aire in the emergence of Foxp3^{lo} T_{reg}P. Furthermore, Aire regulates the pool of recirculating CCR6^{+} T_{reg} throughout life. Interestingly, CCR6^{+} T_{reg} from *Aire*^{KO} mice expressed reduced levels of several genes associated with their polarization and suppressive functions.

Importantly, they express normal levels of *Foxp3*, indicating that they remain engaged in the T_{reg} cell lineage. In accordance with the defective suppressive signature of CCR6$^+$ T_{reg} from *Aire*^{KO} mice, we found that the adoptive transfer of these cells failed to attenuate the severity of multiorgan autoimmunity. In contrast to their thymic counterparts, splenic T_{reg} of *Aire*^{KO} mice show a protection similar to *Aire*^{WT} splenic T_{reg}, consistently with their normal suppressive signature. Altogether, these results indicate that Aire is crucial for the suppressive functions of recirculating CCR6$^+$ T_{reg} in the thymus.

Although Aire is expressed by a subset of recirculating thymic B cells (9), we found that its absence in hematopoietic cells had no impact neither in T_{reg} development nor in CCR6$^+$ T_{reg} recirculation and suppressive signature. Considering the weak expression of *Aire* in thymic B cells compared to mTEC, it is not surprising that *Aire* deficiency in hematopoietic cells does not control the cellularity and suppressive signature of CCR6$^+$ T_{reg}. In marked contrast, beyond controlling the recirculation of CCR6$^+$ T_{reg}, BM chimeras in *Aire*^{KO} recipients revealed that *Aire* expression in stromal cells is responsible for their highly suppressive phenotype.

Interestingly, recirculating Foxp3$^+$ T_{reg} were observed in close proximity to Aire$^+$ mTEC, similarly to developing Foxp3$^+$ T_{reg}. The reduced expression of *Ccl20* and *Cxcl12*, likely responsible for the lower amount of recirculating T_{reg} in these mice as previously reported (5, 8), could contribute to a lesser stimulation of recirculating T_{reg} by mTEC. However, *in vitro* co-culture experiments suggest that defective chemoattraction is unlikely responsible for the phenotype observed in *Aire*^{KO} mice. Furthermore, *in vitro* co-culture assays revealed that Aire$^+$ mTEC were capable to activate peripheral T_{reg} in an antigen-specific manner. Our results suggest that peripheral T_{reg} could regulate *de novo* T_{reg} development not only by competing for IL-2 (5, 57) but also for the cognate self-antigen. In the absence of Aire, *in vitro* co-culture assays and *in vivo* adoptive transfer experiments demonstrate that recirculating T_{reg} activation and suppressive signature were altered. Therefore, our results unravel that Aire$^+$ mTEC control the activated and differentiated phenotype of recirculating T_{reg} upon their entry into the thymus. A possible explanation could be that Aire controls co-stimulation signals that are responsible for the effector phenotype of recirculating T_{reg}. In addition, Aire could also modulate indirectly CCR6$^+$ T_{reg} suppressive properties through other mechanisms such as the medullary positioning of XCR1$^+$ type 1 conventional dendritic cells by controlling the production of the chemokine XCL1 (11). Moreover, further investigations are required to determine the fate of CCR6$^+$ T_{reg} in the thymic medulla. Three possibilities can be envisaged: CCR6$^+$ T_{reg} (1) become long-term resident cells, (2) migrate back to the periphery or (3) die by apoptosis.

This study ameliorates our understanding on recirculating T_{reg} in the thymus, which remain poorly described to date. In summary, it identifies that Aire controls the suppressive properties of recirculating $CCR6^+$ T_{reg} in the thymus. It also assigns a new role for Aire in conferring to mTEC the aptitude to restimulate recirculating T_{reg}. Thus, this study furthers our understanding on the mechanisms allowing recirculating T_{reg} to fine-tune *de novo* T_{reg} production. Finally, our results are expected to contribute to a better understanding in T_{reg} deficiencies observed in the human pathology APECED.

Acknowledgements

We are grateful to Georg Holländer (University of Basel, Switzerland) and Bernard Malissen (CIML, Marseille, France) for providing us *Aire*^{KO} and Foxp3^{eGFP} mice, respectively. We thank the CIML flow cytometry, histology, PICSL imaging facility of the CIML (ImagImm) and animal facility platforms for technical support. We thank Cloé Zamit (CIML, France) for help with mouse genotyping.

Author contributions

JC, AB, JCS, LC, and MI conducted the experiments, analyzed and interpreted the data. MG and AS analyzed the data. JC, AB, JCS and MI wrote the manuscript. MI initiated, supervised and conceived the study.

Funding

This work was supported by institutional grants from INSERM, CNRS and Aix-Marseille Université. The Immune Tolerance and T-Cell Differentiation laboratory received funding from the ARC Foundation (PJA20171206491 to M.I.), CoPoC-proof of concept (MAT-PI-17326-A-01 to M.I.), a prematuration grant from A*MIDEX, a French "Investissements d'avenir" program (LTalpha-Treg to M.I.) and Agence Nationale de la Recherche (grant ANR-19-CE18-0021-01, *RANKLthym* to M.I.). We also acknowledge financial support from France Bio Imaging (ANR-10-INBS-04-01) and France Génomique national infrastructure, funded as part of the "Investissements d'Avenir" program managed by the ANR (ANR-10-INBS-0009). J.C. and A.B. were supported by a PhD fellowship from the Ministère de l'Enseignement Supérieur et de la Recherche et de l'Innovation (MESRI).

Data availability

All data generated or analyzed during this study are included in this published article and its supplementary information files. The dataset generated in this study are available in the Gene Expression Omnibus (GEO) database under accession number GSE188419.

Code availability

Not applicable

Declarations

Conflict of interests

The authors declare that they have no conflict if interest.

Ethical approval

All experiments were done in accordance with national and European laws for laboratory animal welfare (EEC Council Directive 2010/63/UE) and the Marseille Ethical Committee for Animal experimentation.

Consent to participate

Not applicable.

Consent to publication

Not applicable.

References

1. Owen DL, Mahmud SA, Sjaastad LE, Williams JB, Spanier JA, Simeonov DR, et al. Thymic regulatory T cells arise via two distinct developmental programs. Nat Immunol. 2019;20(2):195-205.

2. Lio CW, Hsieh CS. A two-step process for thymic regulatory T cell development. Immunity. 2008;28(1):100-11.

3. Santamaria JC, Borelli A, Irla M. Regulatory T Cell Heterogeneity in the Thymus: Impact on Their Functional Activities. Front Immunol. 2021;12:643153.

4. Marshall D, Sinclair C, Tung S, Seddon B. Differential requirement for IL-2 and IL-15 during bifurcated development of thymic regulatory T cells. J Immunol. 2014;193(11):5525-33.

5. Thiault N, Darrigues J, Adoue V, Gros M, Binet B, Perals C, et al. Peripheral regulatory T lymphocytes recirculating to the thymus suppress the development of their precursors. Nature immunology. 2015.

6. Cowan JE, McCarthy NI, Anderson G. CCR7 Controls Thymus Recirculation, but Not Production and Emigration, of Foxp3(+) T Cells. Cell Rep. 2016;14(5):1041-8.

7. Yang E, Zou T, Leichner TM, Zhang SL, Kambayashi T. Both retention and recirculation contribute to long-lived regulatory T-cell accumulation in the thymus. Eur J Immunol. 2014;44(9):2712-20.

8. Cowan JE, Baik S, McCarthy NI, Parnell SM, White AJ, Jenkinson WE, et al. Aire controls the recirculation of murine Foxp3(+) regulatory T-cells back to the thymus. European journal of immunology. 2018;48(5):844-54.

9. Yamano T, Nedjic J, Hinterberger M, Steinert M, Koser S, Pinto S, et al. Thymic B Cells Are Licensed to Present Self Antigens for Central T Cell Tolerance Induction. Immunity. 2015.

10. Aricha R, Feferman T, Scott HS, Souroujon MC, Berrih-Aknin S, Fuchs S. The susceptibility of Aire(-/-) mice to experimental myasthenia gravis involves alterations in regulatory T cells. J Autoimmun. 2011;36(1):16-24.

11. Lei Y, Ripen AM, Ishimaru N, Ohigashi I, Nagasawa T, Jeker LT, et al. Aire-dependent production of XCL1 mediates medullary accumulation of thymic dendritic cells and contributes to regulatory T cell development. The Journal of experimental medicine. 2011;208(2):383-94.

12. Malchow S, Leventhal DS, Lee V, Nishi S, Socci ND, Savage PA. Aire Enforces Immune Tolerance by Directing Autoreactive T Cells into the Regulatory T Cell Lineage. Immunity. 2016;44(5):1102-13.

13. Yang S, Fujikado N, Kolodin D, Benoist C, Mathis D. Immune tolerance. Regulatory T cells generated early in life play a distinct role in maintaining self-tolerance. Science. 2015;348(6234):589-94.

14. Anderson MS, Venanzi ES, Klein L, Chen Z, Berzins SP, Turley SJ, et al. Projection of an immunological self shadow within the thymus by the aire protein. Science. 2002;298(5597):1395-401.

15. Jiang W, Anderson MS, Bronson R, Mathis D, Benoist C. Modifier loci condition autoimmunity provoked by Aire deficiency. The Journal of experimental medicine. 2005;202(6):805-15.

16. Kuroda N, Mitani T, Takeda N, Ishimaru N, Arakaki R, Hayashi Y, et al. Development of autoimmunity against transcriptionally unrepressed target antigen in the thymus of Aire-deficient mice. J Immunol. 2005;174(4):1862-70.

17. Ramsey C, Winqvist O, Puhakka L, Halonen M, Moro A, KV§mpe O, et al. Aire deficient mice develop multiple features of APECED phenotype and show altered immune response. Hum Mol Genet. 2002;11(4):397-409.

18. Consortium. F-GA. An autoimmune disease, APECED, caused by mutations in a novel gene featuring two PHD-type zinc-finger domains. Nature genetics. 1997;17(4):399-403.

19. Nagamine K, Peterson P, Scott HS, Kudoh J, Minoshima S, Heino M, et al. Positional cloning of the APECED gene. Nat Genet. 1997;17(4):393-8.

20. Ryan KR, Lawson CA, Lorenzi AR, Arkwright PD, Isaacs JD, Lilic D. CD4+CD25+ T-regulatory cells are decreased in patients with autoimmune polyendocrinopathy candidiasis ectodermal dystrophy. J Allergy Clin Immunol. 2005;116(5):1158-9.

21. Kekäläinen E, Tuovinen H, Joensuu J, Gylling M, Franssila R, Pöntynen N, et al. A defect of regulatory T cells in patients with autoimmune polyendocrinopathy-candidiasis-ectodermal dystrophy. J Immunol. 2007;178(2):1208-15.

22. Laakso SM, Laurinolli TT, Rossi LH, Lehtoviita A, Sairanen H, Perheentupa J, et al. Regulatory T cell defect in APECED patients is associated with loss of naive FOXP3(+) precursors and impaired activated population. J Autoimmun. 2010;35(4):351-7.

23. Sansom SN, Shikama-Dorn N, Zhanybekova S, Nusspaumer G, Macaulay IC, Deadman ME, et al. Population and single-cell genomics reveal the Aire dependency, relief from Polycomb silencing, and distribution of self-antigen expression in thymic epithelia. Genome Res. 2014.

24. Shinkai Y, Rathbun G, Lam KP, Oltz EM, Stewart V, Mendelsohn M, et al. RAG-2-deficient mice lack mature lymphocytes owing to inability to initiate V(D)J rearrangement. Cell. 1992;68(5):855-67.

25. Wang Y, Kissenpfennig A, Mingueneau M, Richelme S, Perrin P, Chevrier S, et al. Th2 lymphoproliferative disorder of LatY136F mutant mice unfolds independently of TCR-MHC engagement and is insensitive to the action of Foxp3+ regulatory T cells. J Immunol. 2008;180(3):1565-75.

26. Barnden MJ, Allison J, Heath WR, Carbone FR. Defective TCR expression in transgenic mice constructed using cDNA-based alpha- and beta-chain genes under the control of heterologous regulatory elements. Immunol Cell Biol. 1998;76(1):34-40.

27. Kurts C, Heath WR, Carbone FR, Allison J, Miller JF, Kosaka H. Constitutive class I-restricted exogenous presentation of self antigens in vivo. J Exp Med. 1996;184(3):923-30.

28. Kim D, Pertea G, Trapnell C, Pimentel H, Kelley R, Salzberg SL. TopHat2: accurate alignment of transcriptomes in the presence of insertions, deletions and gene fusions. Genome Biol. 2013;14(4):R36.

29. Trapnell C, Williams BA, Pertea G, Mortazavi A, Kwan G, van Baren MJ, et al. Transcript assembly and quantification by RNA-Seq reveals unannotated transcripts and isoform switching during cell differentiation. Nat Biotechnol. 2010;28(5):511-5.

30. Trapnell C, Hendrickson DG, Sauvageau M, Goff L, Rinn JL, Pachter L. Differential analysis of gene regulation at transcript resolution with RNA-seq. Nat Biotechnol. 2013;31(1):46-53.

31. Pavlidis P, Noble WS. Matrix2png: a utility for visualizing matrix data. Bioinformatics. 2003;19(2):295-6.

32. Irla M, Guenot J, Sealy G, Reith W, Imhof BA, Serge A. Three-dimensional visualization of the mouse thymus organization in health and immunodeficiency. Journal of immunology. 2013;190(2):586-96.

33. Serge A, Bailly AL, Aurrand-Lions M, Imhof BA, Irla M. For3D: Full Organ Reconstruction in 3D, an Automatized Tool for Deciphering the Complexity of Lymphoid Organs. Journal of immunological methods. 2015.

34. Perniola R. Twenty Years of AIRE. Front Immunol. 2018;9:98.

35. Klug DB, Carter C, Crouch E, Roop D, Conti CJ, Richie ER. Interdependence of cortical thymic epithelial cell differentiation and T-lineage commitment. Proceedings of the National Academy of Sciences of the United States of America. 1998;95(20):11822-7.

36. Fontenot JD, Dooley JL, Farr AG, Rudensky AY. Developmental regulation of Foxp3 expression during ontogeny. The Journal of experimental medicine. 2005;202(7):901-6.

37. Cheng G, Yuan X, Tsai MS, Podack ER, Yu A, Malek TR. IL-2 receptor signaling is essential for the development of Klrg1+ terminally differentiated T regulatory cells. Journal of immunology. 2012;189(4):1780-91.

38. Cretney E, Kallies A, Nutt SL. Differentiation and function of Foxp3(+) effector regulatory T cells. Trends in immunology. 2013;34(2):74-80.

39. Joller N, Lozano E, Burkett PR, Patel B, Xiao S, Zhu C, et al. Treg cells expressing the coinhibitory molecule TIGIT selectively inhibit proinflammatory Th1 and Th17 cell responses. Immunity. 2014;40(4):569-81.

40. Fallarino F, Grohmann U, Hwang KW, Orabona C, Vacca C, Bianchi R, et al. Modulation of tryptophan catabolism by regulatory T cells. Nat Immunol. 2003;4(12):1206-12.

41. Garín MI, Chu CC, Golshayan D, Cernuda-Morollón E, Wait R, Lechler RI. Galectin-1: a key effector of regulation mediated by CD4+CD25+ T cells. Blood. 2007;109(5):2058-65.

42. Frias AB, Jr., Hyzny EJ, Buechel HM, Beppu LY, Xie B, Jurczak MJ, et al. The Transcriptional Regulator Id2 Is Critical for Adipose-Resident Regulatory T Cell Differentiation, Survival, and Function. J Immunol. 2019;203(3):658-64.

43. Sawant DV, Vignali DA. Once a Treg, always a Treg? Immunol Rev. 2014;259(1):173-91.

44. Peligero-Cruz C, Givony T, Sebé-Pedrós A, Dobeš J, Kadouri N, Nevo S, et al. IL18 signaling promotes homing of mature Tregs into the thymus. Elife. 2020;9.

45. Anderson MS, Venanzi ES, Chen Z, Berzins SP, Benoist C, Mathis D. The cellular mechanism of Aire control of T cell tolerance. Immunity. 2005;23(2):227-39.

46. Gray D, Abramson J, Benoist C, Mathis D. Proliferative arrest and rapid turnover of thymic epithelial cells expressing Aire. J Exp Med. 2007;204(11):2521-8.

47. Mahmud SA, Manlove LS, Schmitz HM, Xing Y, Wang Y, Owen DL, et al. Costimulation via the tumor-necrosis factor receptor superfamily couples TCR signal strength to the thymic differentiation of regulatory T cells. Nat Immunol. 2014;15(5):473-81.

48. Rodewald HR, Paul S, Haller C, Bluethmann H, Blum C. Thymus medulla consisting of epithelial islets each derived from a single progenitor. Nature. 2001;414(6865):763-8.

49. Irla M, Guerri L, Guenot J, Serge A, Lantz O, Liston A, et al. Antigen recognition by autoreactive cd4(+) thymocytes drives homeostasis of the thymic medulla. PLoS One. 2012;7(12):e52591.

50. Lopes N, Serge A, Ferrier P, Irla M. Thymic Crosstalk Coordinates Medulla Organization and T-Cell Tolerance Induction. Front Immunol. 2015;6:365.

51. Lopes N, Boucherit N, Santamaria JC, Provin N, Charaix J, Ferrier P, et al. Thymocytes trigger self-antigen-controlling pathways in immature medullary thymic epithelial stages. Elife. 2022;11.

52. Borelli A, Irla M. Lymphotoxin: from the physiology to the regeneration of the thymic function. Cell Death Differ. 2021;28(8):2305-14.

53. Liston A, Lesage S, Wilson J, Peltonen L, Goodnow CC. Aire regulates negative selection of organ-specific T cells. Nature immunology. 2003;4(4):350-4.

54. Cowan JE, Parnell SM, Nakamura K, Caamano JH, Lane PJ, Jenkinson EJ, et al. The thymic medulla is required for Foxp3+ regulatory but not conventional CD4+ thymocyte development. The Journal of experimental medicine. 2013;210(4):675-81.

55. Aschenbrenner K, D'Cruz LM, Vollmann EH, Hinterberger M, Emmerich J, Swee LK, et al. Selection of Foxp3+ regulatory T cells specific for self antigen expressed and presented by Aire+ medullary thymic epithelial cells. Nat Immunol. 2007;8(4):351-8.

56. Malchow S, Leventhal DS, Nishi S, Fischer BI, Shen L, Paner GP, et al. Aire-dependent thymic development of tumor-associated regulatory T cells. Science. 2013;339(6124):1219-24.

57. Weist BM, Kurd N, Boussier J, Chan SW, Robey EA. Thymic regulatory T cell niche size is dictated by limiting IL-2 from antigen-bearing dendritic cells and feedback competition. Nat Immunol. 2015;16(6):635-41.

Legends

Fig. 1 The medullary topology is dynamic throughout life, independently of *Aire* expression.

A-C Representative images of thymic sections stained for keratin 14 (red) and counterstained with DAPI (blue) (upper panel). For3D reconstruction of thymic lobes from 9-day- (**A**), 6-week- (**B**) and 1-year-old (**C**) $Aire^{WT}$ and $Aire^{KO}$ mice, using Matlab (middle panel) and Imaris to depict medullary regions according to their volumes from cyan (smallest) to magenta (largest) (lower panel). Axes are graduated in millimeters (mm). Scale bar, 1 mm. The asterisk denotes the central medulla.

D,E Histograms show the number of medullary islets (**D**) and the total medullary volume (**E**) derived from two thymic lobes for each condition.

F The graph shows the volumes of each medullary islet derived from two thymic lobes for each condition from individual mice measured by For3D. The dashed circle denotes the central medulla of each lobe. Horizontal lines represent the geometric mean and SD. ****$p < 0.0001$ using Kruskal-Wallis test for (**F**).

Fig. 2 Developing CCR6$^-$ and recirculating CCR6$^+$ T$_{reg}$ are reduced in *Aire*^{KO} mice throughout life.

A Flow cytometry profiles, frequencies and numbers of CD25$^+$ T$_{reg}$P, Foxp3^{lo} T$_{reg}$P and CD25$^+$Foxp3$^+$ T$_{reg}$ analyzed in CD4$^+$ SP thymocytes from the thymus of 5-day-old *Aire*^{WT} and *Aire*^{KO} mice. The data are derived from 3 independent experiments (n=2-4 mice per group and per experiment).

B,C Frequencies and numbers of CD25$^+$ T$_{reg}$P, Foxp3^{lo} T$_{reg}$P and CD25$^+$Foxp3$^+$ T$_{reg}$ in the thymus of 6-week- (**B**) and 1-year- (**C**) old *Aire*^{WT} and *Aire*^{KO} mice.

D,E Flow cytometry profiles (**D**), frequencies and numbers (**E**) of CCR6$^-$ and CCR6$^+$ cells in CD25$^+$Foxp3$^+$ T$_{reg}$ from 6-week- and 1-year-old *Aire*^{WT} and *Aire*^{KO} mice. The data are derived from at least 3 independent experiments (n=3-4 mice per group and per experiment).

(**F**) The expression of *Ccl20* and *Cxcl12* was measured by qPCR in purified mTEC^{hi} (EpCAM$^+$UEA-1$^+$Ly51$^{-/lo}$CD80^{hi}) from 6-week-old *Aire*^{WT} and *Aire*^{KO} mice.

Bar graphs show ± SEM, *$p < 0.05$, **$p < 0.01$, ***$p < 0.001$, ****$p < 0.0001$ using unpaired Student's t-test (**A, B, C, E**) and two-tailed Mann-Whitney test for (**F**).

Fig. 3 The suppressive signature of recirculating CCR6$^+$ T$_{reg}$ is impaired in the thymus of *Aire*^{KO} mice.

A The expression level of *Foxp3, Klrg1, Il10, Gzmb, Fasl, Lag3, Entpd1 and Nt5e* was measured by qPCR in thymic CCR6$^+$ T$_{reg}$ from 6-week-old *Aire*^{WT} (n=6) and *Aire*^{KO} (n=9) mice. Bar graphs show mean ± SEM, *$p < 0.05$, **$p < 0.01$, ***$p < 0.001$ using two-tailed Mann-Whitney test.

B Scatterplot representations of log10 gene expression levels (FPKM) in recirculating CCR6$^+$ T$_{reg}$ from *Aire*^{WT} and *Aire*^{KO} mice. For representation purposes, expression values of genes below 0.01 were assigned to 0.01. Genes with fold difference > 2 and *p*-adj < 0.05 were considered as up- or down-regulated genes (red and green dots, respectively). RNA-seq was performed on 2 independent biological replicates derived from two mice.

C Heatmap of selected genes down-regulated in recirculating CCR6$^+$ *Aire*^{KO} T$_{reg}$ (Fold Change > 2) compared to their CCR6$^+$ *Aire*^{WT} counterparts and involved in T$_{reg}$ suppressive functions, T$_{reg}$ Th-like, helper T cell polarization, fat and muscle T$_{reg}$. Two biological replicates are shown for each condition.

Fig. 4 The adoptive transfer of recirculating CCR6$^+$ T$_{reg}$ of the *Aire*^{KO} thymus fails to protect from multi-organ autoimmunity.

A Experimental setup: *Rag2*^{KO} recipients were adoptively transferred with CD4$^+$CD25$^+$ T$_{reg}$-depleted CD45.1 WT splenocytes. Four weeks later, they were injected with splenic T$_{reg}$ or thymic CCR6$^+$ T$_{reg}$ derived from *Aire*^{WT} or *Aire*^{KO} mice. Three weeks after T$_{reg}$ adoptive transfer, peripheral tissues were examined for immune infiltration by histology and quantified by flow cytometry. *Rag2*^{KO} recipients injected only with CD4$^+$CD25$^+$ T$_{reg}$-depleted CD45.1 WT splenocytes were used as controls.

B-E Representative photographies of peripheral tissue sections derived from mice transferred with splenic T$_{reg}$ (**B**) or thymic CCR6$^+$ T$_{reg}$ (**D**) and counterstained with hematoxylin/eosin. Diagrams represent organ infiltration levels by CD45.1 donor cells measured by flow cytometry upon splenic T$_{reg}$ (**C**) or thymic CCR6$^+$ T$_{reg}$ (**E**) transfer. Infiltration levels were normalized to the infiltration observed in controls. Dark and light violet in diagram represent high and low infiltrations. Each diagram represents one individual mouse. Scale bar, 150µm for (**B**), 500µm for (**D**).

F,G Sera from mice transferred with CCR6$^+$ T$_{reg}$ were tested for the presence of autoantibodies (green) against pancreas (**F**) and salivary glands (**G**) of *Rag2*^{KO} mice. Nuclei were counterstained with DAPI (blue). Secondary antibodies (II Abs) alone were used as controls. Scale bar, 1 mm. Histograms show mean fluorescence intensity for each condition. Data are derived from 2 to 3 independent experiments (n=3-5 mice per group and per experiment). Bar graphs show mean ± SEM, ****$p < 0.0001$ using unpaired Student's *t* test for (**F**, **G**).

Fig. 5 *Aire* deficiency in the thymic stroma impairs the recirculation and the suppressive signature of CCR6$^+$ T$_{reg}$.

A Experimental setup: lethally irradiated CD45.2 *Aire*^{WT} or *Aire*^{KO} recipients were reconstituted with BM cells from CD45.1 Foxp3^{eGFP} mice. Six weeks later, thymic T$_{reg}$ subsets of CD45.1 origin were analyzed by flow cytometry. CCR6$^+$ T$_{reg}$ were cell-sorted to measure the expression levels of genes associated with their suppressive functions.

B Flow cytometry profiles, frequencies and numbers of CD4$^+$ SP thymocytes of CD45.1 origin in the thymus of BM chimeric mice.

C, D Flow cytometry profiles and numbers of CD25$^+$ T$_{reg}$P, Foxp3^{lo} T$_{reg}$P and total CD25$^+$Foxp3$^+$ cells (**C**) as well as of CCR6$^-$ and CCR6$^+$ cells in CD25$^+$Foxp3$^+$ T$_{reg}$ (**D**) of CD45.1 origin in the thymus of BM chimeras. Data are derived from 2 independent experiments (n=4 mice per group and per experiment).

E The expression level of *Foxp3, Klrg1, Il10, Tgfb1, Gzmb, Fasl, Lag3, Entpd1* and *Nt5e* was measured by qPCR in purified CCR6^{+}CD25^{+}Foxp3^{+} T_{reg} from CD45.1 Foxp3^{eGFP} →*Aire*^{WT} (n=8) and CD45.1 Foxp3^{eGFP}→*Aire*^{KO} (n=9) chimeras. Data are derived from 2 independent experiments (n=4-5 mice per group and per experiment). Bar graphs show mean ± SEM, *p < 0.05, **p < 0.01, ***p < 0.001, ****p < 0.0001 using unpaired Student's *t* test for (**B-D**) and two-tailed Mann-Whitney test for (**E**).

Fig. 6. Aire^{+} mTEC control the activation and suppressive signature of recirculating T_{reg} through antigen-dependent contact.

A The expression level of *Tgfb1, Gzmb, Fasl, Entpd1* and *Nt5e* was measured by qPCR in splenic T_{reg} from *Aire*^{WT} or *Aire*^{KO} mice co-cultured with *Aire*^{WT} or *Aire*^{KO} mTEC. Data are derived from 2 independent experiments.

B Experimental setup: purified splenic T_{reg} from CD45.1 Foxp3^{eGFP} mice were adoptively transferred *i.v.* into sublethally irradiated CD45.2 *Aire*^{WT} or *Aire*^{KO} recipients. Adoptively transferred CD45.1 Foxp3^{eGFP} T_{reg} were cell-sorted from the thymus of recipient mice one week later and their suppressive signature was analyzed by qPCR.

C Flow cytometry profiles, frequencies and numbers of CD45.1 Foxp3^{eGFP} donor T_{reg} observed in the thymus of CD45.2 *Aire*^{WT} or *Aire*^{KO} recipients.

D The expression level of *Il10, Tgfb1, Gzmb, Fasl, Lag3* and *Nt5e* was measured by qPCR in CD45.1 Foxp3^{eGFP} donor T_{reg} transferred into *Aire*^{WT} (n=4) or *Aire*^{KO} (n=4) recipients.

E Representative images of WT thymic sections stained for Aire (green), Foxp3 (red) and CD73 (white). Yellow and white arrowheads denote developing CD73^{-} and recirculating CD73^{+} T_{reg}, respectively. Scale bar, 30µm.

F Flow cytometry profiles of CD69 activation of splenic OTII T_{reg} from Rip-mOVA x OTII x *Rag2*^{KO} mice co-cultured with $OVA_{323-339}$-loaded *Aire*^{het} (*Aire*$^{eGFP/WT}$) or *Aire*^{KO} (*Aire*$^{eGFP/eGFP}$) mTEC^{hi} after 24h later. The histogram shows the frequencies of CD69^{+} T_{reg} normalized to the activation of OTII T_{reg} co-cultured with *Aire*^{het} mTEC^{hi}.

G The expression level of *Il10, Tgfb1, Gzmb, Fasl, Lag3, Entpd1* and *Nt5e* was measured by qPCR in splenic OTII T_{reg} from Rip-mOVA x OTII x *Rag2*^{KO} mice co-cultured with $OVA_{323-339}$-loaded *Aire*^{het} (*Aire*$^{eGFP/WT}$; n=6) or *Aire*^{KO} (*Aire*$^{eGFP/eGFP}$; n=6) mTEC^{hi}.

Data are derived from 2 independent experiments. Bar graphs show mean ± SEM, *p < 0.05, **p < 0.01, ***p < 0.001 and ****p < 0.0001 using two-tailed Mann-Whitney test for (**A, C, D, F, G**).

Fig. S1 Gating strategy used to purify recirculating CCR6$^+$ T$_{reg}$ in the thymus.

CD4$^+$CD25$^+$ cells were identified in CCR6$^+$CD4$^+$ T cells and analyzed for Foxp3 expression by flow cytometry.

Fig. S2 The suppressive signature of thymic CCR6$^+$ T$_{reg}$ from 1-year-old *Aire*^{KO} mice is altered.

The expression level of *Foxp3*, *Klrg1*, *Il10*, *Gzmb*, *Fasl*, *Entpd1* and *Nt5e* was measured by qPCR in thymic CCR6$^+$ T$_{reg}$ from 1-year-old *Aire*^{WT} (n=5-6) and *Aire*^{KO} (n=9) mice. Bar graphs show mean ± SEM, ns>0.05, ***p<0.001, ****p<0.0001 using two-tailed Mann-Whitney test.

Fig. S3 Splenic *Aire*^{KO} T$_{reg}$ show a normal suppressive signature throughout life.

A, B Flow cytometry profiles, frequencies and numbers of CD4$^+$Foxp3$^+$ T$_{reg}$ in the blood of 6 week- (**A**) and 1-year-old (**B**) *Aire*^{WT} and *Aire*^{KO} mice.

C, D Flow cytometry profiles, frequencies and numbers of CD4$^+$Foxp3$^+$ T$_{reg}$ in the spleen of 6-week- (**C**) and 1-year- old (**D**) *Aire*^{WT} or *Aire*^{KO} mice. Data are derived from 2 independent experiments (n=2-5 mice per group and per experiment).

E, F The expression level of *Foxp3*, *Il10*, *Tgfb1*, *Gzmb*, *Fasl*, *Lag3*, *Entpd1 and Nt5e* was measured by qPCR in splenic T$_{reg}$ from 6-week- (**E**) and 1-year- (**F**) old *Aire*^{WT} (n=4-9 for 6 wk and n=8-13 for 1 yr) and *Aire*^{KO} (n=5-9 for 6 wk and n=8-13 for 1 yr) mice. Bar graphs show mean ± SEM, *p<0.05 and **p<0.01 using unpaired Student's *t* test for (**C, D**).

Fig. S4 The adoptive transfer of thymic CCR6$^+$ T$_{reg}$ from *Aire*^{KO} mice fail to attenuate peripheral tissue infiltration.

A Gating strategy used to sort CCR6$^+$CD4$^+$CD8$^-$CD25$^+$ cells, corresponding to CCR6$^+$ T$_{reg}$ from the thymus of 6-week-old *Aire*^{WT} and *Aire*^{KO} mice.

B Flow cytometry profiles and numbers of CD45.2 donor T$_{reg}$ in inguinal lymph nodes.

C Flow cytometry profiles, frequencies and numbers of CD45.1 infiltrating cells in the pancreas, eyes and salivary glands.

D Flow cytometry profiles and numbers of CD4$^+$ and CD8$^+$ T cells of CD45.1 origin infiltrating the pancreas, eyes and salivary glands. Data are derived from 3 independent experiments (n=2-5 mice per group and per experiment).

Bar graphs show mean ± SEM, *p<0.05, **p<0.01, ***p<0.001 and ****p<0.0001 using two-tailed Mann-Whitney test for (**B**) or using unpaired Student's *t* test for (**C,D**).

Fig. S5 *Aire* expression in hematopoietic cells does not control the recirculation and suppressive signature of thymic CCR6$^+$ T$_{reg}$.

A Experimental setup: Lethally irradiated CD45.1/2 WT recipients were reconstituted with CD45.2 *Aire*^{WT} or *Aire*^{KO} BM cells. Six weeks later, the recirculation and the suppressive signature of thymic CCR6$^+$ T$_{reg}$ of CD45.2 origin were analyzed by flow cytometry and qPCR, respectively.

B,C Flow cytometry profiles, frequencies and numbers of total B220$^+$CD19$^+$ B cells (**B**) and of IgD$^-$ or IgD$^+$ cells in B220$^+$CD19$^+$ B cells (**C**).

D,E Flow cytometry profiles, frequencies and numbers of CD25$^+$ T$_{reg}$P, Foxp3^{lo} T$_{reg}$P and CD25$^+$Foxp3$^+$ T$_{reg}$ (**D**) as well as CCR6$^-$ and CCR6$^+$ cells in total CD25$^+$Foxp3$^+$ T$_{reg}$ (**E**).

F The expression level of *Foxp3*, *Klrg1*, *Il10*, *Gzmb*, *Fasl*, *Lag3*, *Entpd1* and *Nt5e* was measured by qPCR in CCR6$^+$ T$_{reg}$ of CD45.2 origin purified from the thymus of *Aire*^{WT} (n=8) and *Aire*^{KO} (n=8) BM chimeric mice. Data are derived from 2 independent experiments (n=4 mice per group and per experiment). Bar graphs show mean ± SEM, *p<0.05 using two-tailed Mann-Whitney test.

Fig. S6 Gating strategy used to purify Aire$^+$ mTEC^{hi}.

Aire$^+$ mTEC^{hi} were identified as EpCAM$^+$Ly51$^{-/lo}$CD80$^+$Aire^{eGFP} cells and purified from *Aire*^{het} (Aire$^{eGFP/WT}$) and *Aire*^{KO} (Aire$^{eGFP/eGFP}$) mice.

Fig. S7 *Aire*^{KO} mTEC express reduced levels of OX40L and GITRL.

A Representative flow cytometry profiles of MHCII in mTEC from *Aire*^{WT} and *Aire*^{KO} mice. The histogram shows the frequency of MCHII$^+$ mTEC. Bar graphs show mean ± SEM, **p<0.001 using two-tailed Mann-Whitney.

B-C *Aire*^{KO} mTEC express reduced levels of OX40L and GITRL. Expression levels of *Tnfsf4* (OX40L) and *Tnfsf18* (GITRL) measured by RNA-seq **(B)** and flow cytometry **(C)** in *Aire*^{WT} and *Aire*^{KO} mTEC^{hi}. Bar graphs show mean ± SEM, **p<0.01 using two-tailed Mann-Whitney test.

Table S1. FPKM values of RNA-seq data derived from thymic CCR6$^+$ Treg from *Aire*^{WT} and *Aire*^{KO} mice.

Table S2. List of antibodies used for flow cytometry.

Table S3. List of primers used for RT-qPCR.

Movie S1. 3D rotation of *Aire*^{WT} thymic lobe of 9-day-old mouse, with medullary compartment colored according to their volume.

Aire^{WT} thymic lobe (DAPI, blue) of a 9-day-old mouse is rendered in 3D with medullary compartments (Keratin 14, pseudo-colors) encoded according to medullary volumes from cyan (smallest medullae) to magenta (largest medullae). All axes are graduated with 500-µm grid spacing.

Movie S2. 3D rotation of *Aire*^{KO} thymic lobe of 9-day-old mouse, with medullary compartment colored according to their volume.

Aire^{KO} thymic lobe (DAPI, blue) of a 9-day-old mouse is rendered in 3D with medullary compartments (Keratin 14, pseudo-colors) encoded according to medullary volumes from cyan (smallest medullae) to magenta (largest medullae). All axes are graduated with 500-µm grid spacing.

Movie S3. 3D rotation of *Aire*^{WT} thymic lobe of 6-week-old mouse, with medullary compartment colored according to their volume.

Aire^{WT} thymic lobe (DAPI, blue) of a 6-week-old mouse is rendered in 3D with medullary compartments (Keratin 14, pseudo-colors) encoded according to medullary volumes from cyan (smallest medullae) to magenta (largest medullae). All axes are graduated with 500-µm grid spacing.

Movie S4. 3D rotation of *Aire*^{KO} thymic lobe of 6-week-old mouse, with medullary compartment colored according to their volume.

Aire^{KO} thymic lobe (DAPI, blue) of a 6-week-old mouse is rendered in 3D with medullary compartments (Keratin 14, pseudo-colors) encoded according to medullary volumes from cyan (smallest medullae) to magenta (largest medullae). All axes are graduated with 500-µm grid spacing.

Movie S5. 3D rotation of *Aire*^{WT} thymic lobe of 1-year-old mouse, with medullary compartment colored according to their volume.

736 *Aire*^{WT} thymic lobe (DAPI, blue) of a 1-year-old mouse is rendered in 3D with medullary compartments (Keratin
737 14, pseudo-colors) encoded according to medullary volumes from cyan (smallest medullae) to magenta (largest
738 medullae). All axes are graduated with 500-µm grid spacing.

739 **Movie S6. 3D rotation of *Aire*^{KO} thymic lobe of 1-year-old mouse, with medullary compartment colored**
740 **according to their volume.**

741 *Aire*^{KO} thymic lobe (DAPI, blue) of a 1-year-old mouse is rendered in 3D with medullary compartments (Keratin
742 14, pseudo-colors) encoded according to medullary volumes from cyan (smallest medullae) to magenta (largest
743 medullae). All axes are graduated with 500-µm grid spacing.

Figure 1

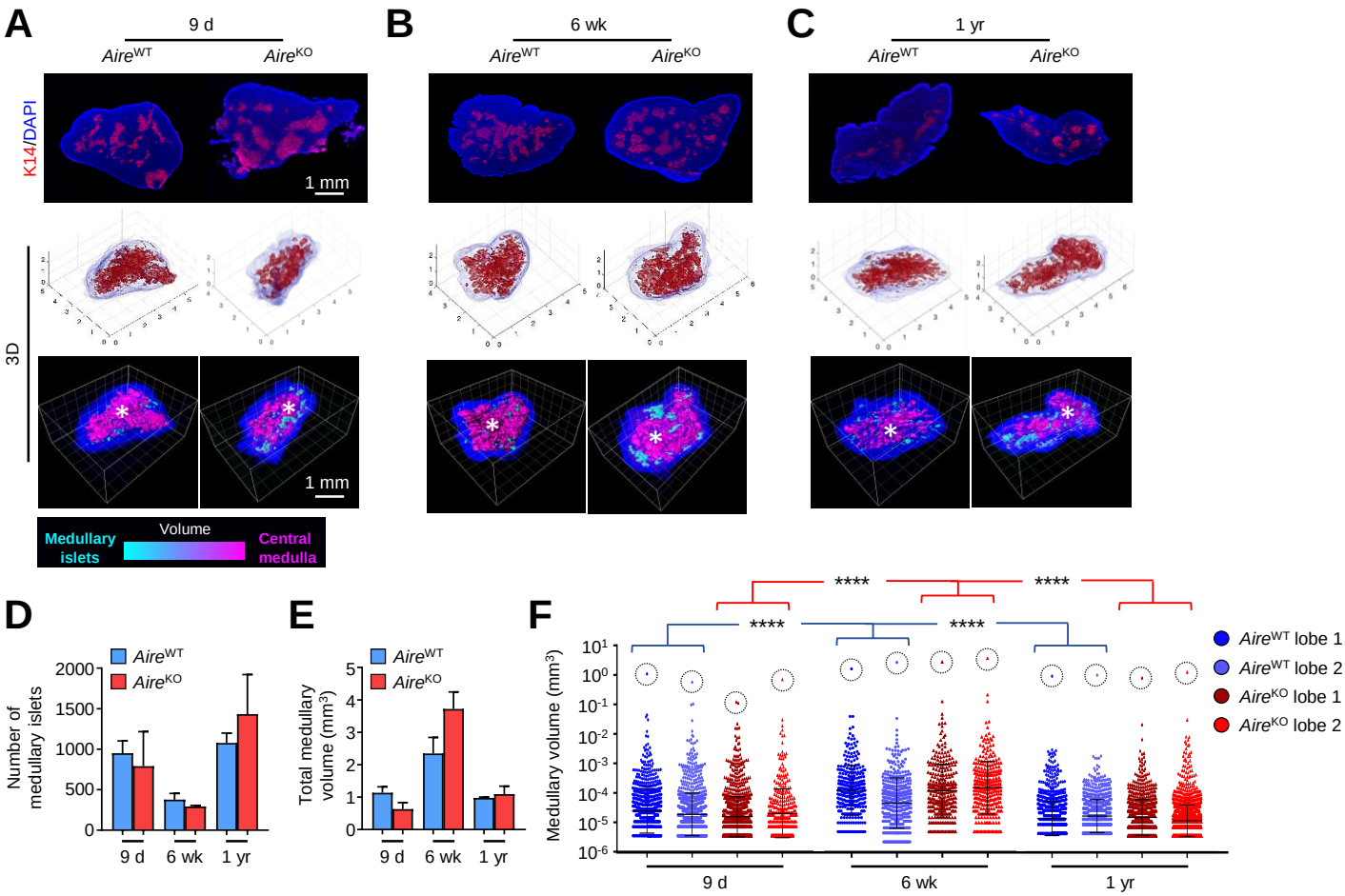
A
9 d
Aire^WT
Aire^KO
B
6 wk
Aire^WT
Aire^KO
C
1 yr
Aire^WT
Aire^KO
K14/DAPI
1 mm
3D
1 mm
Medullary islets
Volume
Central medulla
D
Number of medullary islets
2000
1500
1000
500
0
Aire^WT
Aire^KO
9 d
6 wk
1 yr
E
Total medullary volume (mm^3)
5
4
3
2
1
0
Aire^WT
Aire^KO
9 d
6 wk
1 yr
F
Medullary volume (mm^3)
10^1
10^0
10^-1
10^-2
10^-3
10^-4
10^-5
10^-6
****
****
****
****
9 d
6 wk
1 yr
Aire^WT lobe 1
Aire^WT lobe 2
Aire^KO lobe 1
Aire^KO lobe 2

Figure 2

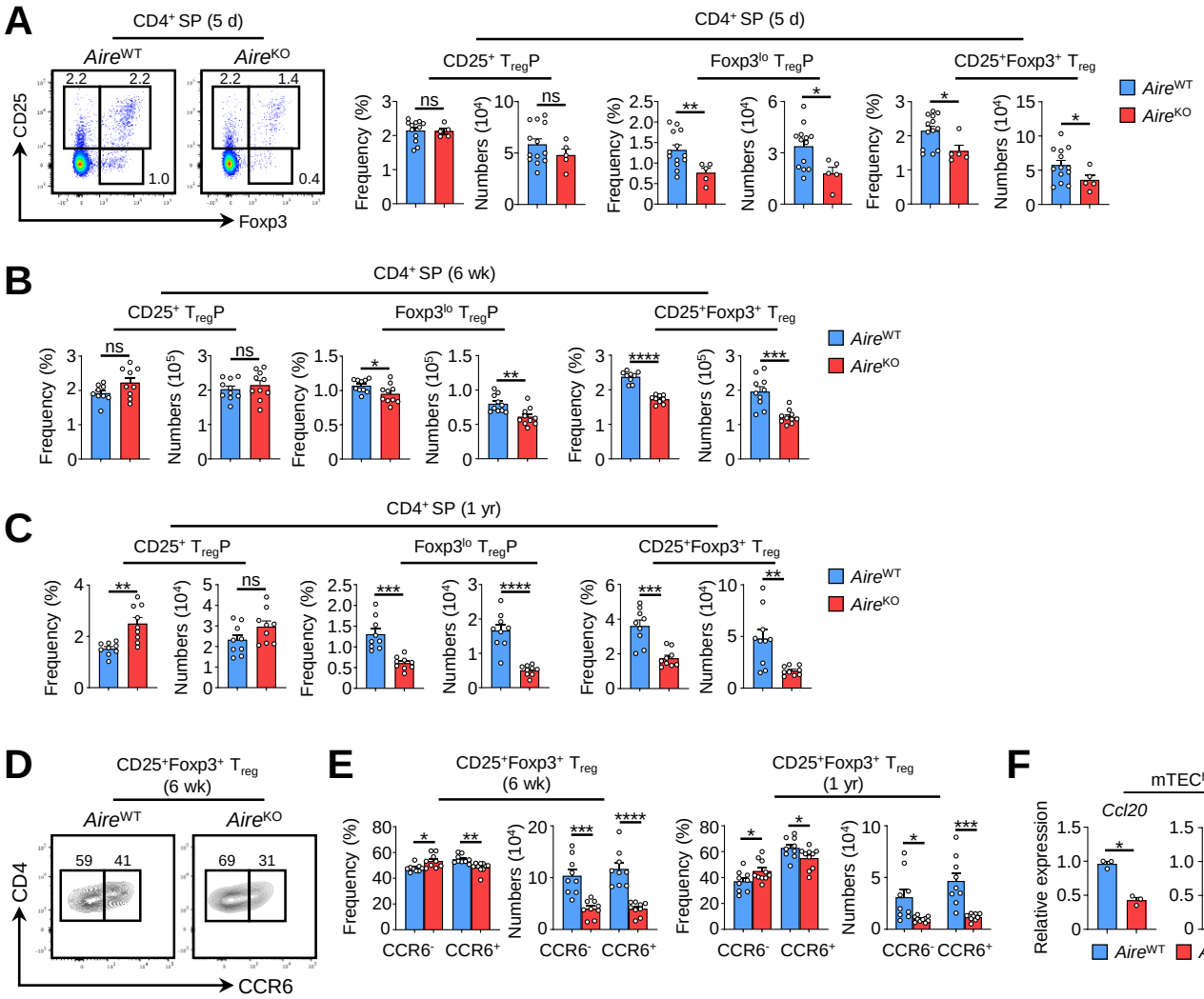
A
CD4+ SP (5 d)
AireWT
AireKO
CD25
Foxp3
2.2
2.2
1.0
2.2
1.4
0.4
CD4+ SP (5 d)
CD25+ TregP
Foxp3lo TregP
CD25+Foxp3+ Treg
Frequency (%)
Numbers (10^4)
ns
**
*
AireWT
AireKO
B
CD4+ SP (6 wk)
CD25+ TregP
Foxp3lo TregP
CD25+Foxp3+ Treg
Frequency (%)
Numbers (10^5)
ns
*
**
****
***
AireWT
AireKO
C
CD4+ SP (1 yr)
CD25+ TregP
Foxp3lo TregP
CD25+Foxp3+ Treg
Frequency (%)
Numbers (10^4)
**
ns
***
****
AireWT
AireKO
D
CD25+Foxp3+ Treg (6 wk)
AireWT
AireKO
CD4
CCR6
59
41
69
31
E
CD25+Foxp3+ Treg (6 wk)
CD25+Foxp3+ Treg (1 yr)
Frequency (%)
Numbers (10^4)
CCR6-
CCR6+
F
mTEChi
Ccl20
Cxcl12
Relative expression
AireWT
AireKO

Figure 3

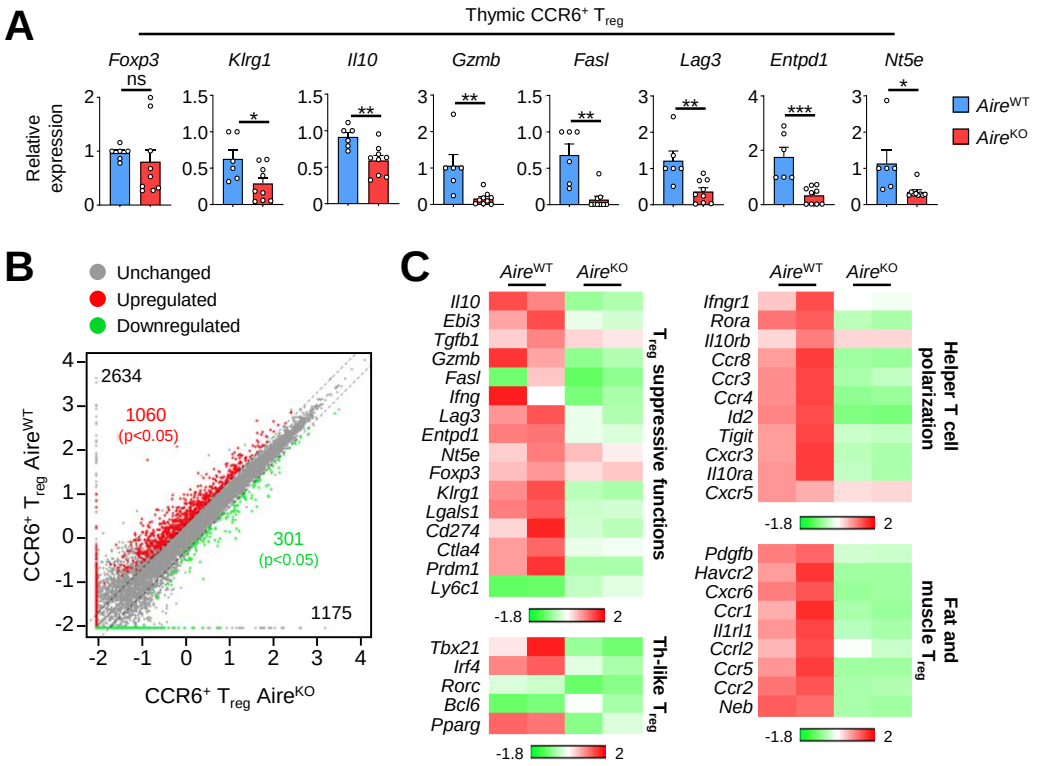
A
Thymic CCR6+ Treg
Foxp3
Klrg1
Il10
Gzmb
Fasl
Lag3
Entpd1
Nt5e
ns
Relative expression
AireWT
AireKO
B
Unchanged
Upregulated
Downregulated
2634
1060
(p<0.05)
301
(p<0.05)
1175
CCR6+ Treg AireWT
CCR6+ Treg AireKO
C
AireWT
AireKO
Il10
Ebi3
Tgfb1
Gzmb
Fasl
Ifng
Lag3
Entpd1
Nt5e
Foxp3
Klrg1
Lgals1
Cd274
Ctla4
Prdm1
Ly6c1
Treg suppressive functions
Tbx21
Irf4
Rorc
Bcl6
Pparg
Th-like Treg
Ifngr1
Rora
Il10rb
Ccr8
Ccr3
Ccr4
Id2
Tigit
Cxcr3
Il10ra
Cxcr5
Helper T cell polarization
Pdgfb
Havcr2
Cxcr6
Ccr1
Il1rl1
Ccrl2
Ccr5
Ccr2
Neb
Fat and muscle Treg
-1.8
2

Figure 4

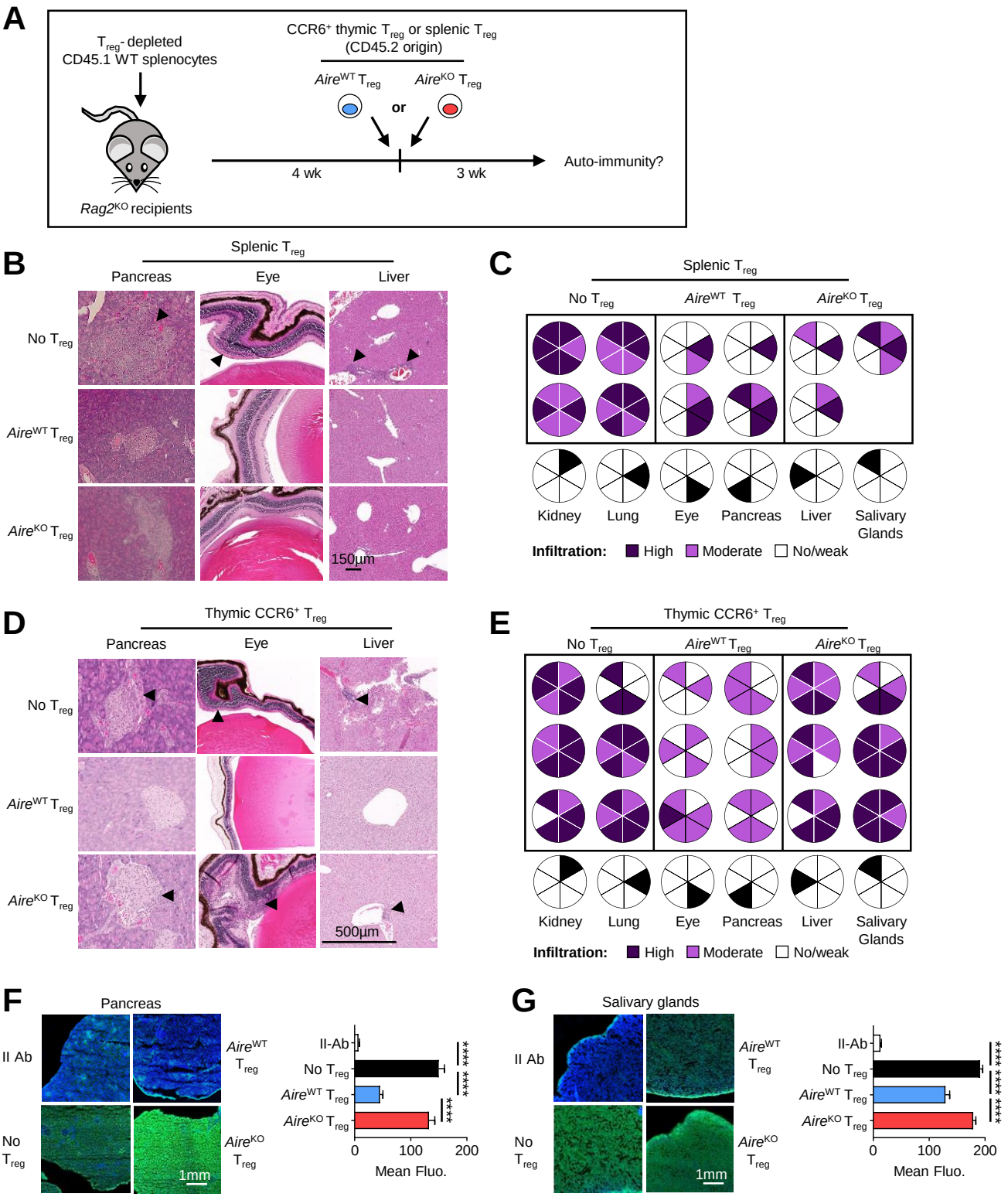
A
Treg- depleted
CD45.1 WT splenocytes
Rag2KO recipients
CCR6+ thymic Treg or splenic Treg
(CD45.2 origin)
AireWT Treg
or
AireKO Treg
4 wk
3 wk
Auto-immunity?
B
Splenic Treg
Pancreas
Eye
Liver
No Treg
AireWT Treg
AireKO Treg
150µm
C
Splenic Treg
No Treg
AireWT Treg
AireKO Treg
Kidney
Lung
Eye
Pancreas
Liver
Salivary Glands
Infiltration:
High
Moderate
No/weak
D
Thymic CCR6+ Treg
Pancreas
Eye
Liver
No Treg
AireWT Treg
AireKO Treg
500µm
E
Thymic CCR6+ Treg
No Treg
AireWT Treg
AireKO Treg
Kidney
Lung
Eye
Pancreas
Liver
Salivary Glands
Infiltration:
High
Moderate
No/weak
F
Pancreas
II Ab
No Treg
AireWT Treg
AireKO Treg
1mm
II-Ab
No Treg
AireWT Treg
AireKO Treg
****
****
***
0
100
200
Mean Fluo.
G
Salivary glands
II Ab
No Treg
AireWT Treg
AireKO Treg
1mm
II-Ab
No Treg
AireWT Treg
AireKO Treg
****
****
***
0
100
200
Mean Fluo.

Figure 5

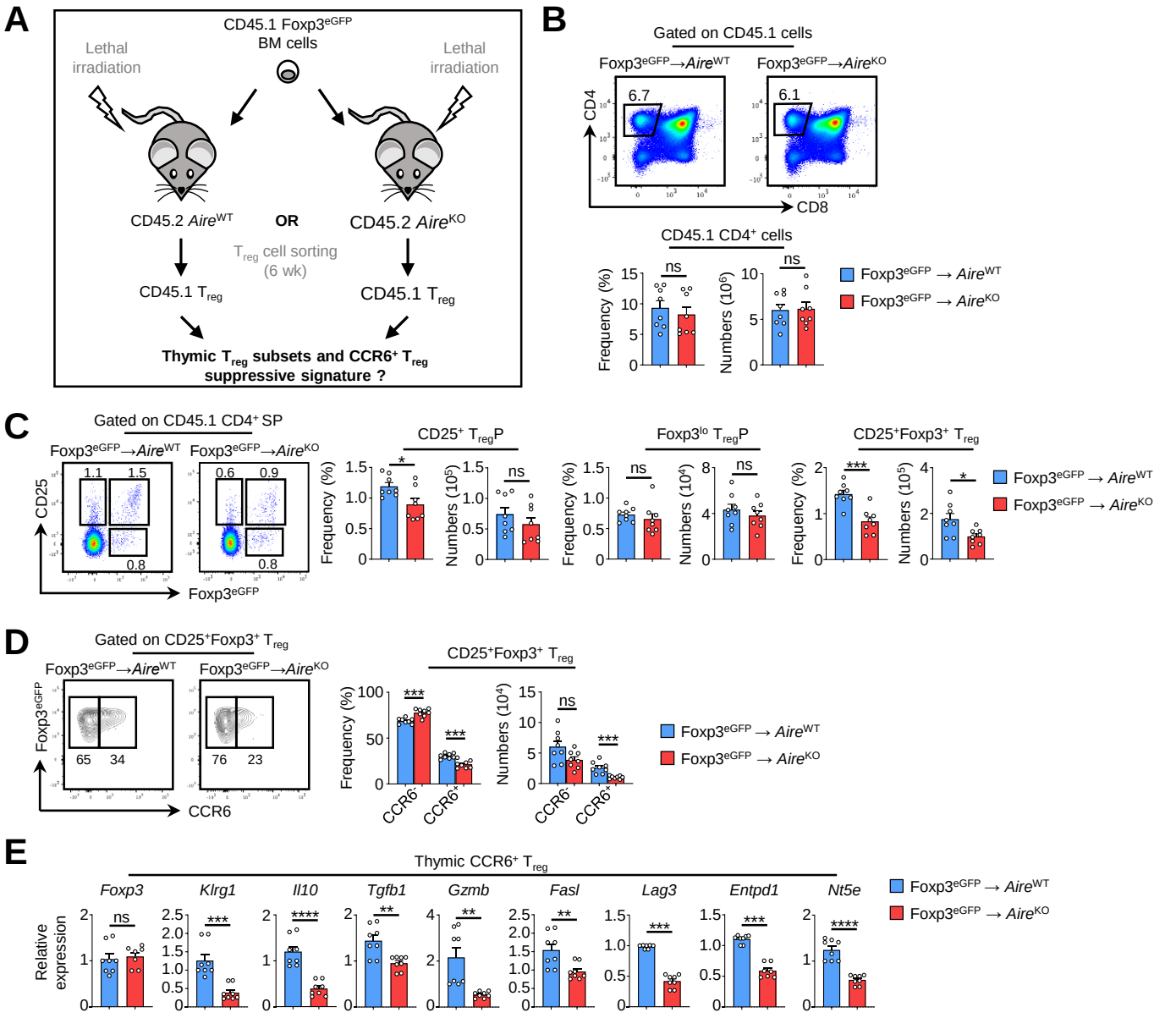
A
CD45.1 Foxp3eGFP BM cells
Lethal irradiation
Lethal irradiation
CD45.2 AireWT
OR
CD45.2 AireKO
Treg cell sorting (6 wk)
CD45.1 Treg
CD45.1 Treg
Thymic Treg subsets and CCR6+ Treg suppressive signature ?
B
Gated on CD45.1 cells
Foxp3eGFP→AireWT
Foxp3eGFP→AireKO
6.7
6.1
CD4
CD8
CD45.1 CD4+ cells
Frequency (%)
Numbers (10^6)
ns
ns
Foxp3eGFP → AireWT
Foxp3eGFP → AireKO
C
Gated on CD45.1 CD4+ SP
Foxp3eGFP→AireWT
Foxp3eGFP→AireKO
CD25
Foxp3eGFP
1.1
1.5
0.8
0.6
0.9
0.8
CD25+ TregP
Foxp3lo TregP
CD25+Foxp3+ Treg
Frequency (%)
Numbers (10^5)
Numbers (10^4)
*
ns
***
Foxp3eGFP → AireWT
Foxp3eGFP → AireKO
D
Gated on CD25+Foxp3+ Treg
Foxp3eGFP→AireWT
Foxp3eGFP→AireKO
Foxp3eGFP
CCR6
65
34
76
23
CD25+Foxp3+ Treg
Frequency (%)
Numbers (10^4)
***
ns
CCR6-
CCR6+
Foxp3eGFP → AireWT
Foxp3eGFP → AireKO
E
Thymic CCR6+ Treg
Foxp3
Klrg1
Il10
Tgfb1
Gzmb
Fasl
Lag3
Entpd1
Nt5e
Relative expression
ns
***
****
**
Foxp3eGFP → AireWT
Foxp3eGFP → AireKO

Figure 6

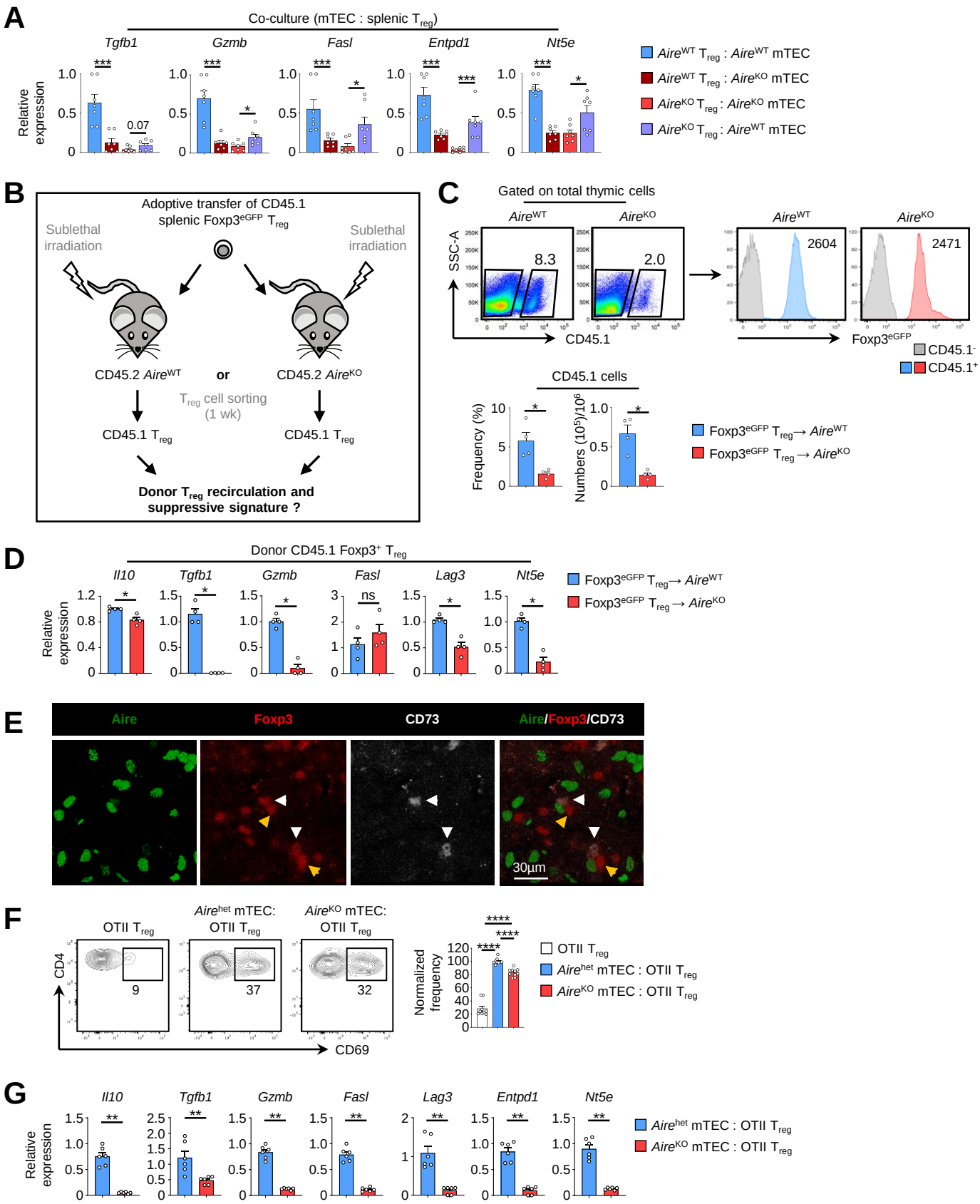
A
Co-culture (mTEC : splenic Treg)
Tgfb1
Gzmb
Fasl
Entpd1
Nt5e
Relative expression
0.07
Aire^WT Treg : Aire^WT mTEC
Aire^WT Treg : Aire^KO mTEC
Aire^KO Treg : Aire^KO mTEC
Aire^KO Treg : Aire^WT mTEC
B
Adoptive transfer of CD45.1 splenic Foxp3^eGFP Treg
Sublethal irradiation
Sublethal irradiation
CD45.2 Aire^WT
or
CD45.2 Aire^KO
Treg cell sorting (1 wk)
CD45.1 Treg
CD45.1 Treg
Donor Treg recirculation and suppressive signature ?
C
Gated on total thymic cells
Aire^WT
Aire^KO
SSC-A
8.3
2.0
CD45.1
2604
2471
Foxp3^eGFP
CD45.1-
CD45.1+
CD45.1 cells
Frequency (%)
Numbers (10^5)/10^6
Foxp3^eGFP Treg→ Aire^WT
Foxp3^eGFP Treg→ Aire^KO
D
Donor CD45.1 Foxp3+ Treg
Il10
Tgfb1
Gzmb
Fasl
Lag3
Nt5e
Relative expression
ns
Foxp3^eGFP Treg→ Aire^WT
Foxp3^eGFP Treg→ Aire^KO
E
Aire
Foxp3
CD73
Aire/Foxp3/CD73
30µm
F
OTII Treg
Aire^het mTEC: OTII Treg
Aire^KO mTEC: OTII Treg
CD4
CD69
9
37
32
Normalized frequency
OTII Treg
Aire^het mTEC : OTII Treg
Aire^KO mTEC : OTII Treg
G
Il10
Tgfb1
Gzmb
Fasl
Lag3
Entpd1
Nt5e
Relative expression
Aire^het mTEC : OTII Treg
Aire^KO mTEC : OTII Treg

Fig. S1

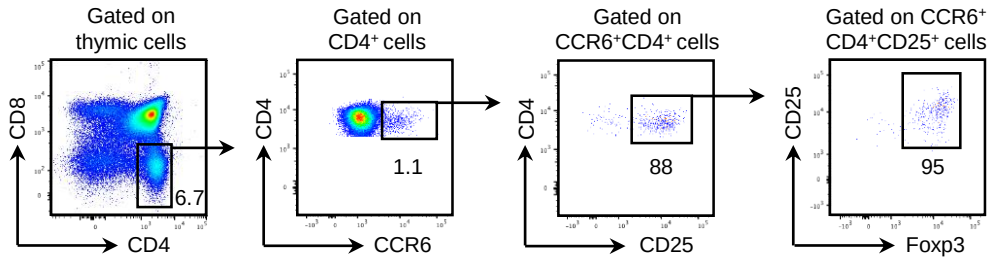
Gated on
thymic cells
CD8
CD4
6.7
Gated on
CD4+ cells
CD4
CCR6
1.1
Gated on
CCR6+CD4+ cells
CD4
CD25
88
Gated on CCR6+
CD4+CD25+ cells
CD25
Foxp3
95

Fig. S2

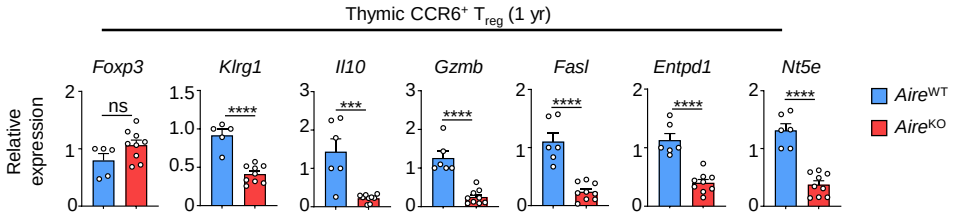
Thymic CCR6+ Treg (1 yr)
Foxp3
Klrg1
Il10
Gzmb
Fasl
Entpd1
Nt5e
Relative expression
ns
****
***
AireWT
AireKO

Fig. S3

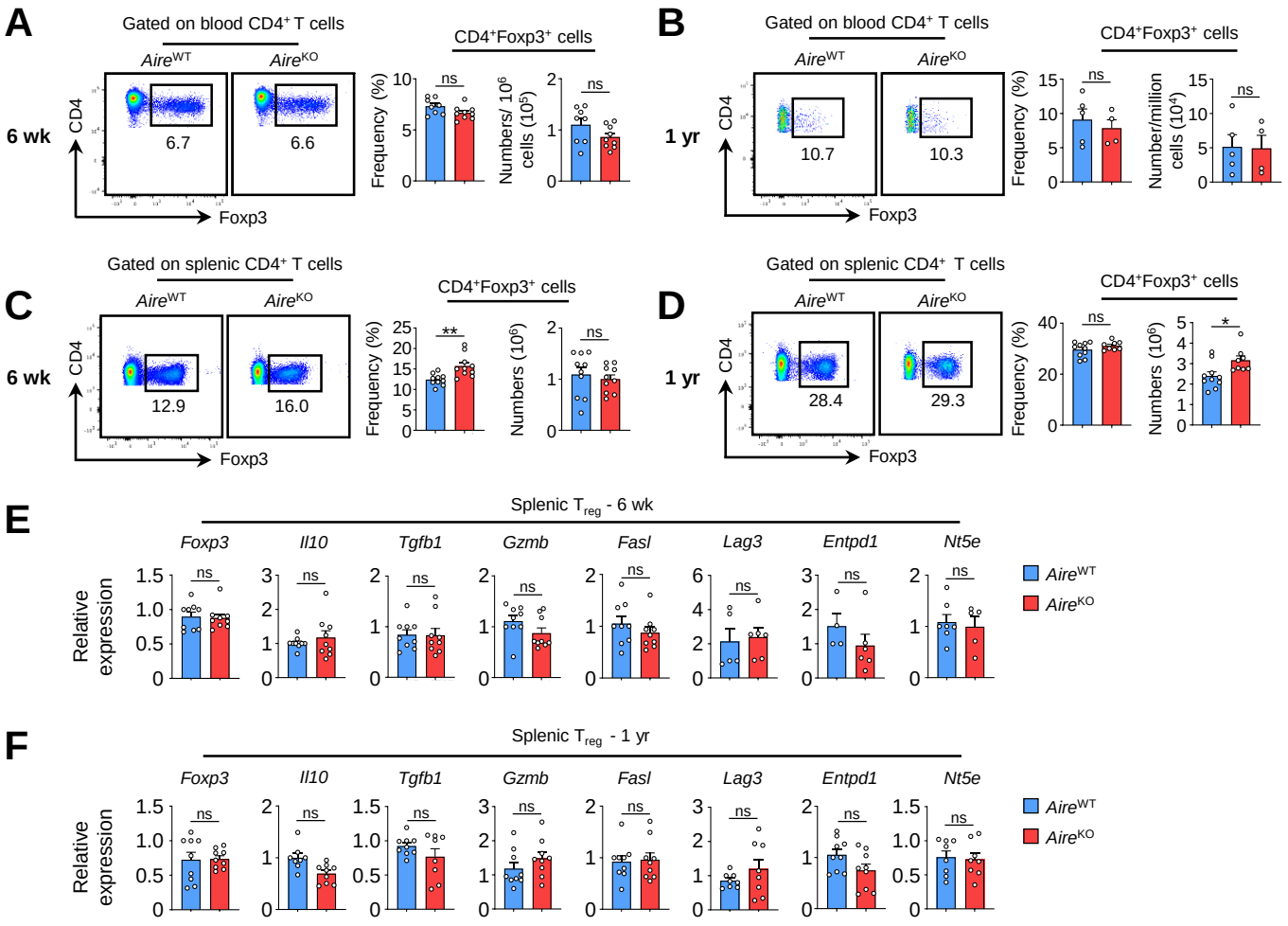
A
Gated on blood CD4+ T cells
AireWT
AireKO
6 wk
CD4
Foxp3
6.7
6.6
CD4+Foxp3+ cells
Frequency (%)
Numbers/ 10^6 cells (10^5)
ns
B
Gated on blood CD4+ T cells
1 yr
10.7
10.3
Number/million cells (10^4)
C
Gated on splenic CD4+ T cells
12.9
16.0
Numbers (10^6)
**
D
28.4
29.3
*
E
Splenic Treg - 6 wk
Foxp3
Il10
Tgfb1
Gzmb
Fasl
Lag3
Entpd1
Nt5e
Relative expression
F
Splenic Treg - 1 yr

Fig. S4

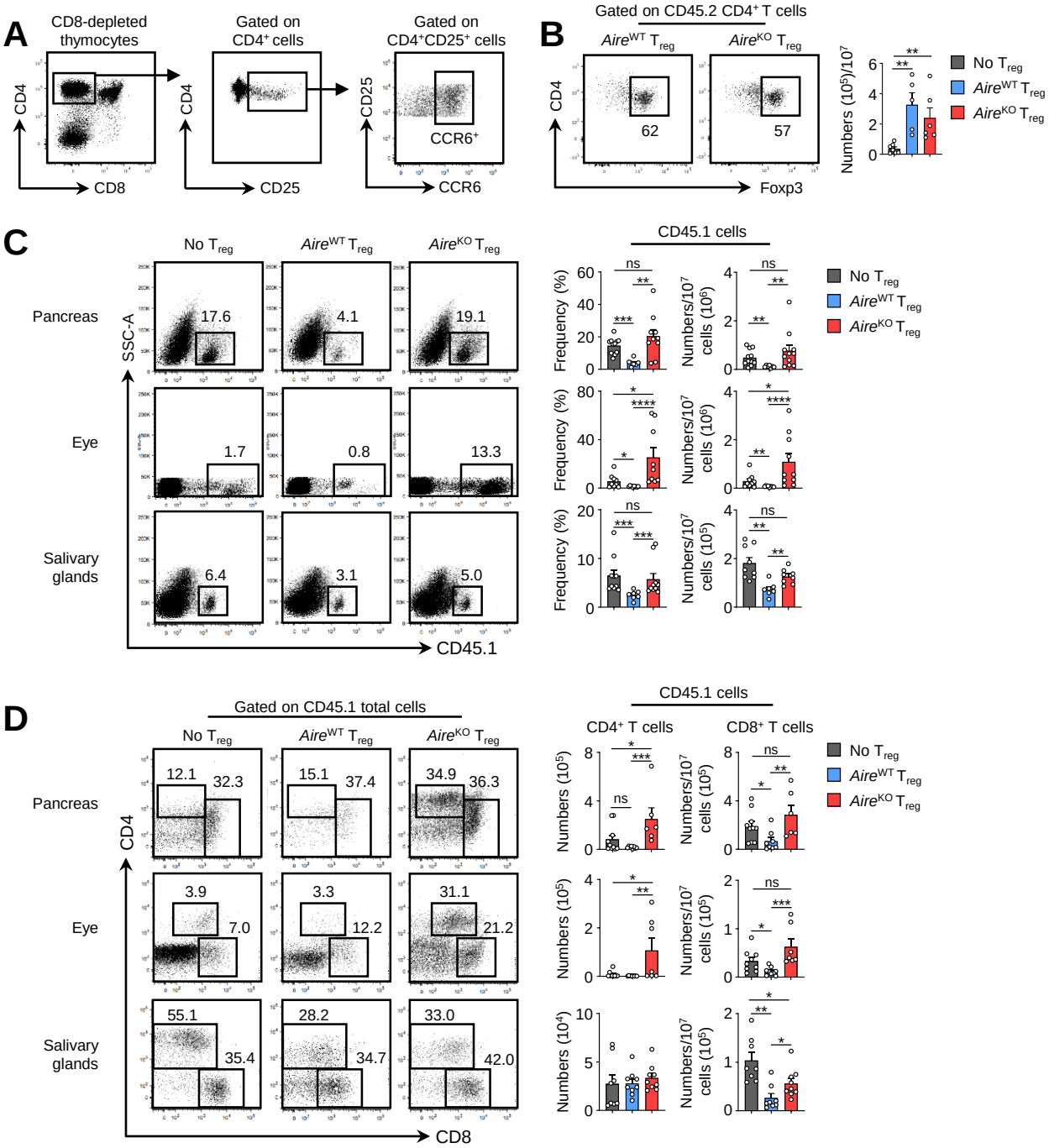
A
CD8-depleted thymocytes
Gated on CD4+ cells
Gated on CD4+CD25+ cells
CD4
CD8
CD25
CCR6
CCR6+
B
Gated on CD45.2 CD4+ T cells
AireWT Treg
AireKO Treg
62
57
Foxp3
Numbers (10^5)/10^7
No Treg
AireWT Treg
AireKO Treg
C
No Treg
AireWT Treg
AireKO Treg
Pancreas
Eye
Salivary glands
SSC-A
17.6
4.1
19.1
1.7
0.8
13.3
6.4
3.1
5.0
CD45.1
CD45.1 cells
Frequency (%)
Numbers/10^7 cells (10^6)
Numbers/10^7 cells (10^5)
D
Gated on CD45.1 total cells
CD4
CD8
12.1
32.3
15.1
37.4
34.9
36.3
3.9
7.0
3.3
12.2
31.1
21.2
55.1
35.4
28.2
34.7
33.0
42.0
CD45.1 cells
CD4+ T cells
CD8+ T cells
Numbers (10^5)
Numbers (10^4)
Numbers/10^7 cells (10^5)

Fig. S5

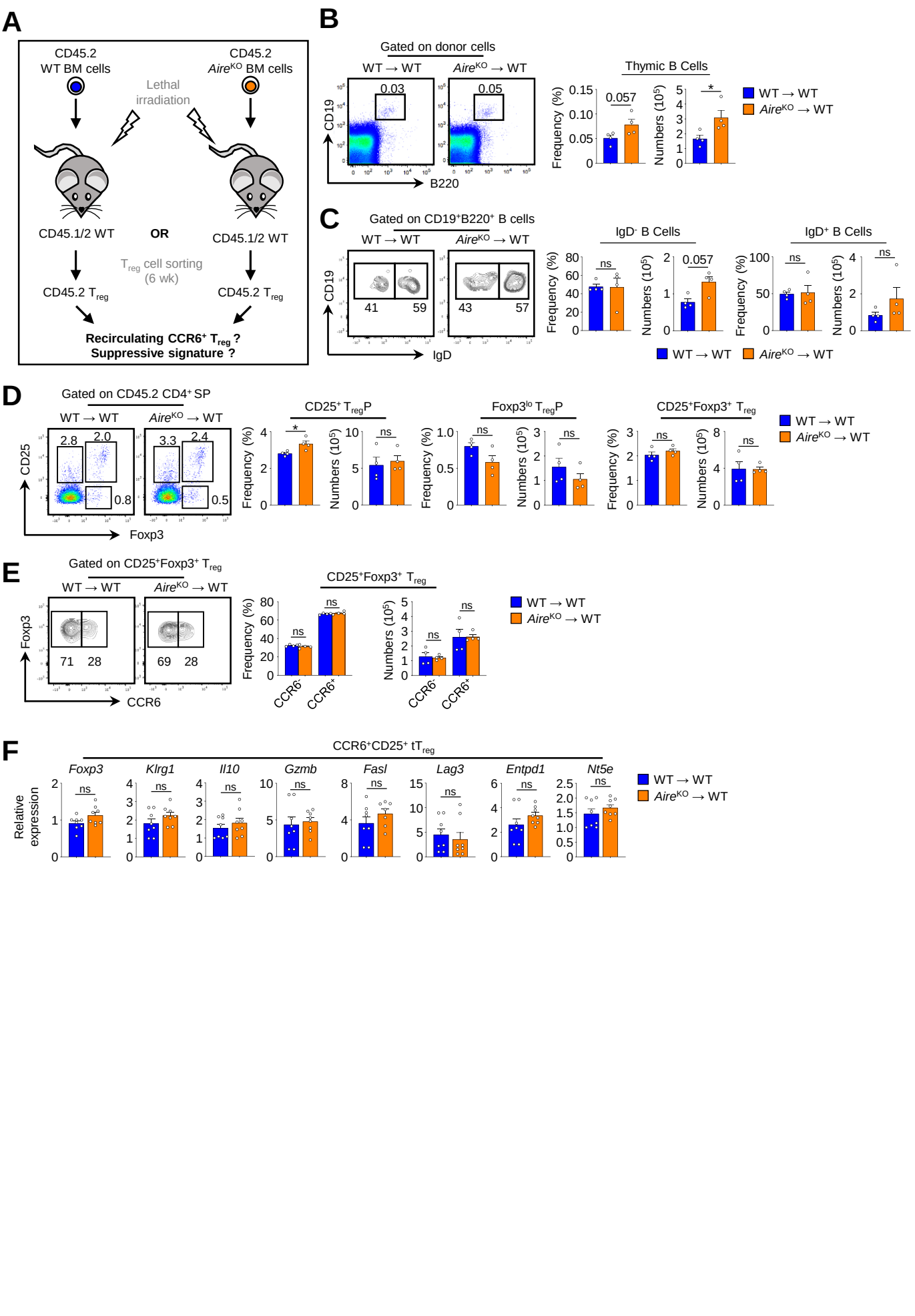
A
CD45.2
WT BM cells
CD45.2
Aire^KO BM cells
Lethal
irradiation
CD45.1/2 WT
OR
CD45.1/2 WT
T_reg cell sorting
(6 wk)
CD45.2 T_reg
CD45.2 T_reg
Recirculating CCR6+ T_reg ?
Suppressive signature ?
B
Gated on donor cells
WT → WT
Aire^KO → WT
CD19
B220
0.03
0.05
Thymic B Cells
Frequency (%)
Numbers (10^5)
0.057
*
WT → WT
Aire^KO → WT
C
Gated on CD19+B220+ B cells
WT → WT
Aire^KO → WT
CD19
IgD
41
59
43
57
IgD- B Cells
IgD+ B Cells
Frequency (%)
Numbers (10^5)
ns
0.057
WT → WT
Aire^KO → WT
D
Gated on CD45.2 CD4+ SP
WT → WT
Aire^KO → WT
CD25
Foxp3
2.8
2.0
0.8
3.3
2.4
0.5
CD25+ T_regP
Foxp3lo T_regP
CD25+Foxp3+ T_reg
Frequency (%)
Numbers (10^5)
*
ns
WT → WT
Aire^KO → WT
E
Gated on CD25+Foxp3+ T_reg
WT → WT
Aire^KO → WT
Foxp3
CCR6
71
28
69
28
CD25+Foxp3+ T_reg
Frequency (%)
Numbers (10^5)
ns
CCR6-
CCR6+
WT → WT
Aire^KO → WT
F
CCR6+CD25+ tT_reg
Foxp3
Klrg1
Il10
Gzmb
Fasl
Lag3
Entpd1
Nt5e
Relative expression
ns
WT → WT
Aire^KO → WT

Fig. S6

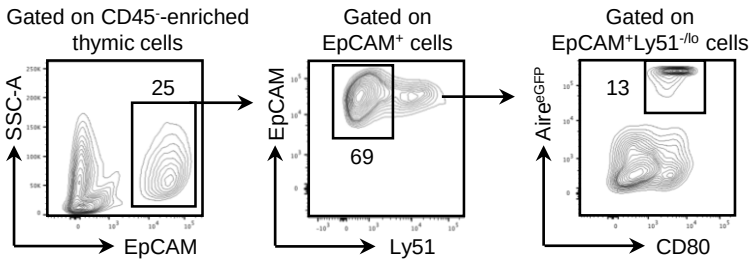
Gated on CD45⁻-enriched thymic cells
25
SSC-A
EpCAM
Gated on EpCAM⁺ cells
69
EpCAM
Ly51
Gated on EpCAM⁺Ly51⁻/lo cells
13
Aire^eGFP
CD80

Fig. S7

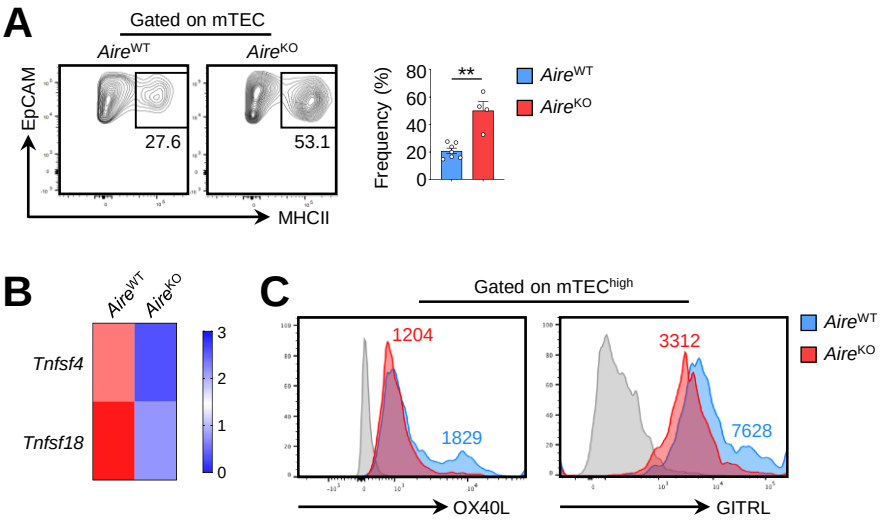
A
Gated on mTEC
Aire^WT
Aire^KO
EpCAM
MHCII
27.6
53.1
Frequency (%)
80
60
40
20
0
**
Aire^WT
Aire^KO
B
Aire^WT
Aire^KO
Tnfsf4
Tnfsf18
3
2
1
0
C
Gated on mTEC^high
1204
1829
3312
7628
OX40L
GITRL
Aire^WT
Aire^KO

Table S1

Gene	*Aire*^{WT} mice	*Aire*^{KO} mice
Il10	3.09 ± 0.44	0.31 ± 0.19
Gzmb	25.57 ± 6.90	4.83 ± 1.84
Fasl	1.35 ± 0.66	0.92 ± 0.15
Lag3	4.29 ± 0.53	2.07 ± 0.45
Entpd1	10.57 ± 0.19	5.43 ± 0.38
Nt5e	69.74 ± 11.42	59.41 ± 7.12
Prdm1	18.78 ± 3.56	2.84 ± 0.06
Klrg1	60.16 ± 9.26	12.96 ± 2.67
Tigit	77.14 ± 16.33	23.54 ± 1.83
Ctla4	259.10 ± 19.43	156.50 ± 2.15
Lgals1	421.5 ± 20.12	244.0 ± 3.59
Tbx21	5.22 ± 1.64	2.2 ± 0.32
Irf4	20.71 ± 1.10	13.22 ± 1.40
Pparg	2.54 ± 0.09	0.87 ± 0.39
Id2	192.5 ± 25.10	34.59 ± 2.99
Cxcr3	58.30 ± 14.08	14.94 ± 2.71
Ccr4	35.47 ± 5.00	11.08 ± 0.12
Ccr8	256.6 ± 35.04	136.7 ± 3.35
Ccr1	3.67 ± 1.31	0.34 ± 0.13
Ccr2	39.94 ± 2.88	7.26 ± 0.64

Table S2

Antibody	Clone	Fluorochrome	Supplier	Dilution
B220	RA3-6B2	PerCP	Biolegend	1/200
CD45.1	A20	BV421	Biolegend	1/600
CD45.1	A20	PerCP Cy5.5	BD Biosciences	1/200
CD45.2	104	AF488	Biolegend	1/200
CD4	RM4.5	FITC	BD Biosciences	1/200
CD4	RM4.5	APC	Biolegend	1/200
CD4	GK1.5	APC Cy7	Invitrogen	1/200
CD4	RM4.5	BV421	BD Biosciences	1/200
CD8α	53.6.7	PeCy7	BD Biosciences	1/600
CD8α	53.6.7	PB	BD Biosciences	1/200
CD25	PC61	PerCP Cy5.5	BD Biosciences	1/200
CD25	PC61	APC	Biolegend	1/200
CD25	PC61	PeCy7	Biolegend	1/400
CCR6	29-2L17	PE	Biolegend	1/300
CCR6	29-2L17	PerCP Cy5.5	Biolegend	1/200
CD44	IM7	PerCP Cy5.5	eBioscience	1/200
CD19	1D3	PeCy7	BD Biosciences	1/300
CD69	H1.2F3	PE	Biolegend	1/300
IA/IE	M5/114.15.2	BV605	BD Biosciences	1/1000
GITRL	YGL386	PE	Biolegend	1/200
OX40L	RM134L	APC	eBioscience	1/200
CD80	16-10A1	PerCP Cy5.5	Biolegend	1/200
EpCAM	G8.8	PeCy7	Biolegend	1/3000
Foxp3	FKJ-16s	PE	eBioscience	1/200
Foxp3	FKJ-16s	APC	Invitrogen	1/200
Foxp3	FKJ-16s	AF488	Invitrogen	1/150
IgD	11-26c.2a	PE	BD Biosciences	1/300
Ly51	6C3	PE	Biolegend	1/3000
UEA1		FITC	Vector Laboratories	1/800

Table S3

Primers	Sequence	Tm (°C)	Amplicon size (bp)	Accesion number
Actin - Forward	CAGAAGGAGATTACTGCTCTGGCT	58.2	93	NM_007393.5
Actin - Reverse	GGAGCCACCGATCCACACA	59.9		
Foxp3 - Forward	CCCACCTACAGGCCCTTCTC	61.1	71	NM_001199347.1 NM_001199348.1 NM_054039.2
Foxp3 - Reverse	GGCATGGGCATCCACAGT	58.4		
Klrg1 - Forward	CGAGGAATGGTAGCCACTGTTAC	57.3	163	NM_016970
Klrg1 - Reverse	CCGATCCAGTAAAAGTCCTGACC	57.1		
Il10 – Forward	GAATTCCCTGGGTGAGAAGC	55.7	105	NM_010548.2
Il10 – Reverse	CTCTTCACCTGCTCCACTGC	58.1		
Gzmb - Forward	GAAAACAATGAAAAGCAGCTAACTACA	56.9	69	NM_013542.3
Gzmb - Reverse	TCTAGGGACGATGGGTAATCAGA	56.3		
Fasl - Forward	TCAGTCTTGCAACAACCAGC	55.9	310	NM_001205243.1 NM_010177
Fasl - Reverse	AGACAATATTCCTGGTGCCC	54.7		
Lag3 - Forward	CTGGGACTGCTTTGGGAAG	55.9	167	NM_008479.2
Lag3 - Reverse	GGTTGATGTTGCCAGATAACCC	56.2		
Entpd1 - Forward	TACCACCCCATCTGGTCATT	55.7	168	NM_001304721.1 NM_009848.4
Entpd1 - Reverse	GGACGTTTTGTTTGGTTGGT	56.0		
Nt5e - Forward	CAAATCCCACACAACCACTG	54.3	158	NM_011851.4
Nt5e - Reverse	TGCTCACTTGGTCACAGGAC	56.9		
Tgfb1 - Forward	CAGACATTCGGGAAGCAGTG	57.9	145	NM_011577.2
Tgfb1 - Reverse	AGCCGGTTACCAAGGTAACG	57.3		